
Electronic Theses and Dissertations, 2004-2019

2008

Integration Of A Nanostructure Embedded Thermoresponsive Polymer For Microfluidic Applications

Ghanashyam Londe
University of Central Florida

 Part of the [Electrical and Electronics Commons](#)
Find similar works at: <https://stars.library.ucf.edu/etd>
University of Central Florida Libraries <http://library.ucf.edu>

This Doctoral Dissertation (Open Access) is brought to you for free and open access by STARS. It has been accepted for inclusion in Electronic Theses and Dissertations, 2004-2019 by an authorized administrator of STARS. For more information, please contact STARS@ucf.edu.

STARS Citation

Londe, Ghanashyam, "Integration Of A Nanostructure Embedded Thermoresponsive Polymer For Microfluidic Applications" (2008). *Electronic Theses and Dissertations, 2004-2019*. 3598.
<https://stars.library.ucf.edu/etd/3598>

INTEGRATION OF A NANOSTRUCTURE EMBEDDED
THERMORESPONSIVE POLYMER FOR MICROFLUIDIC
APPLICATIONS

by

GHANASHYAM LONDE

B.E., B.V.B. College of Engr. & Tech., India, 1999

M.S. University of Central Florida, 2004

A dissertation submitted in partial fulfillment of the requirements
for the degree of Doctor of Philosophy in Electrical Engineering
in the School of Electrical Engineering and Computer Science
in the College of Engineering and Computer Science
at the University of Central Florida
Orlando, Florida

Fall Term
2008

Major Professor: Hyoung Jin Cho

© 2008 Ghanashyam Londe

ABSTRACT

This work describes the modeling, synthesis, integration and characterization of a novel nanostructure embedded thermoresponsive material for microfluidic applications.

The innumerable applications of thermoresponsive surfaces in the recent years have necessitated the development of a rigorous mathematical treatment for these surfaces to understand and improve their behavior. An analytical model is proposed to describe the transfer characteristic (variation of contact angle versus temperature) of a unique switchable, nanostructured, thermoresponsive surface consisting of silica nanoparticles and the thermoresponsive polymer, Poly(N-isopropylacrylamide) (PNIPAAm) which changes its wetting angle upon heating. Important metrics such as the absolute lower critical solution temperature, threshold & saturation temperatures and gain are modeled and quantified by mathematical expressions.

Based on the modeling, a heat source for the thermoresponsive surface was integrated on the glass substrate itself to create a fully functional smart surface. The design and fabrication of a smart platform consisting of the switchable, nanostructured, thermoresponsive surface with an integrated gold microheater for wettability control and its time response analysis was conducted.

The insight gained into the behavior of the thermoresponsive surface by using the analytical model, aided the effort in the effective integration of the surface into a microfluidic channel for flow regulation applications. The implementations of novel microfluidic flow regulator concepts were tested. The aim is to integrate a regulator function to a channel surface utilizing the layer-by-layer (LBL) deposition technique.

The characterization and pressure differential study of the microfluidic regulators was carried out on simple straight microchannels which were selectively coated with the thermoresponsive surface. Theoretical and experimental studies were performed to determine the important characteristic parameters including capillary, Weber and Reynolds numbers. The pressure differential data was used to develop critical operating specifications.

This work lays out a new microfluidic device concept consisting of a channel with a built-in regulatory function.

Dedicated to my advisor Dr. H. J. Cho, my family, friends and coworkers who have supported and inspired me.

ACKNOWLEDGMENTS

This research has been partially supported by the National Science Foundation (ECS 0348603, DMR 0746499) and University of Central Florida (UCF) In-House Support.

TABLE OF CONTENTS

LIST OF FIGURES	x
LIST OF TABLES	xiii
LIST OF ACRONYMS/ABBREVIATIONS	xiv
CHAPTER 1: INTRODUCTION	1
1.1. Research Motivation	1
1.2. Previous Work and Research Objectives	3
CHAPTER 2: ANALYTICAL MODEL FOR THE WETTABILITY SWITCHING CHARACTERISTICS OF NANOSTRUCTURED THERMORESPONSIVE SURFACES	8
2.1. Modeling Contact Angle of Rough Surfaces	8
2.1.1. Wenzel Model	9
2.1.2. Cassie-Baxter Model	9
2.2. Synthesis of Superhydrophobic Surfaces	10
2.3. Switching Characteristics of the Thermoresponsive Surfaces	14
2.4. Analytical Model for the Switching Characteristic of the Thermoresponsive Surface	16
CHAPTER 3: THERMOSENSITIVE SMART SURFACE WITH INTEGRATED MICROHEATER FOR WETTABILITY CONTROL	23
3.1. Design and Fabrication	23
3.2. Results and Discussion	28
3.3. Time Response Analysis	29
CHAPTER 4: MICROFLUIDIC FLOW REGULATION BASED ON SUPERHYDROPHOBIC NANOSTRUCTURES AND SWITCHABLE THERMOSENSITIVE SURFACE	36
4.1. Design	39

4.2.	Fabrication of the Passive Microfluidic Valve with the Superhydrophobic Surface	40
4.2.1.	Microchannel Fabrication	40
4.2.2.	Polyelectrolyte Deposition.....	42
4.2.3.	Polydimethylsiloxane (PDMS) Bonding and Interconnection	42
4.2.4.	Fabrication of the Superhydrophobic surface	43
4.3.	Fabrication of the Microfluidic Valve with the Thermosensitive Polymer	45
4.3.1.	Initial Polyelectrolyte Deposition	45
4.3.2.	Annealing.....	47
4.3.3.	Initiator Deposition	47
4.3.4.	Thermosensitive Polymer (PNIPAAm) and Perfluorosilane Deposition ..	48
4.4.	Test Results and Discussion.....	49
4.4.1.	Passive Microfluidic Valve with Superhydrophobic Surface.....	51
4.4.2.	Microfluidic Valve with the Thermosensitive Polymer.....	54
CHAPTER 5: CHARACTERIZATION OF THE SWITCHABLE THERMORESPONSIVE MICROFLUIDIC FLOW REGULATOR.....		58
5.1.	Device Design.....	58
5.2.	Fluid Mechanics in Microdevices.....	61
5.2.1.	Dimensionless Numbers to Characterize Microflow	61
5.2.2.	Pressure Differential	64
5.2.2.1.	Hagen-Poiseuille Equation.....	65
5.2.2.2.	Young-Laplace Equation	66
5.3.	Measurement Set-up	70
5.3.1.	Calibration of the Pressure Sensor	70
5.3.2.	Differential Pressure Measurement for the Microfluidic Flow Regulator	72

CHAPTER 6: CONCLUSION AND FUTURE WORK	89
APPENDIX A: RCA CLEANING	92
APPENDIX B: GLASS ETCHING FOR MICROCHANNEL FABRICATION	96
APPENDIX C: GLASS-PDMS BONDING USING CORONA TREATER.....	100
REFERENCES	105
PUBLICATIONS AND PRESENTATIONS	113

LIST OF FIGURES

Figure 1.1: Global Nanotechnology Market, 2005-2013	2
Figure 2.1: AFM height images of A, B and C.....	13
Figure 2.2: Plot of contact angle versus surface temperature for surfaces A, B and C	15
Figure 2.3: Plot of the calculated contact angle fitted on the measured contact angle versus surface temperature for surfaces A, B and C.....	18
Figure 2.4: Plot of the first and second differential of the contact angle versus the surface temperature for surface A	20
Figure 2.5: Piece-wise linear approximation method to find the threshold and saturation temperatures to characterize the onset and end of the LCST range.....	21
Figure 3.1: Schematic showing the dimensions of the gold thin film microheater	24
Figure 3.2: Fabrication process for the Thermosensitive Polymer-on-Microheater smart platform.....	26
Figure 3.3: AFM image of the PNIPAAm decorated with silica nanoparticles and the fabricated switchable thermosensitive polymer-on-microheater platform	28
Figure 3.4: Plot of variation of contact angle of a water droplet and variation of temperature of the smart thermoresponsive surface versus voltage applied to the microheater	30
Figure 3.5: Plot of contact angle change of a water droplet on the thermosensitive surface versus time	31
Figure 3.6: Time response of the thermoresponsive smart surface. Plot shows normalized contact angle variation versus time.....	35
Figure 4.1: Schematic of the flow regulator. In-Inlet; O1-Outlet 1; O2-Outlet 2.....	39
Figure 4.2: Fabrication process the passive valve	41

Figure 4.3: Silica nanoparticles on porous multilayered polyelectrolyte surface	44
Figure 4.4: Fabrication process for the thermosensitive valve	46
Figure 4.5: Fabricated structure showing the inlet/outlet reservoirs and the superhydrophobic/hydrophilic polymer film	50
Figure 4.6: SEM micrograph of the cross-section of the etched glass channel with a PDMS seal	50
Figure 4.7: SEM micrograph of switchable thermoresponsive polymer deposited inside etched glass capillary	51
Figure 4.8: Contact angle vs. concentration of water/2-isoproanol mixtures on a polymer surface	52
Figure 4.9: "Closed" status of the passive valve	53
Figure 4.10: "Open" status of the passive valve	53
Figure 4.11: Plot of contact angle vs. temperature on the switchable thermosensitive surface	54
Figure 4.12: Contact angle change with increasing temperature	55
Figure 4.13: "Closed" status of the thermoresponsive valve	56
Figure 4.14: "Open" status of the thermoresponsive valve	57
Figure 5.1: The fabricated straight channel microfluidic device in glass substrate with the integrated switchable, nanostructured, thermoresponsive surface	59
Figure 5.2: SEM micrograph showing trapezoidal cross section of the microchannel	60
Figure 5.3: Shape of the advancing meniscus of the water at the interface of the glass-PNIPAAm contact line	65
Figure 5.4: Schematic depicting the shape of the principal radius of curvature of the advancing meniscus of water in a hydrophobic channel with respect to the width of the channel	68

Figure 5.5: Calibration curve for the pressure sensor	71
Figure 5.6: Schematic showing the set up for the pressure measurement. In, Out - inlet & outlet respectively of the microfluidic device.....	73
Figure 5.7: Picture of the set for pressure measurement.....	74
Figure 5.8: Close up view of the microfluidic device mounted on the heater and connected to the pressure sensor for pressure measurement	75
Figure 5.9: Plot of pressure versus time for the straight channel microfluidic device with the integrated thermoresponsive surface at 55 °C.....	77
Figure 5.10: Schematic of the changing radius of curvature of the advancing meniscus of water flowing under capillary action in the microchannel.....	82
Figure 5.11: Variation of surface tension pressure differential and contact angle of the integrated thermoresponsive surface in the microfluidic flow regulator	85
Figure 5.12: Plot of pressure versus time for the straight channel microfluidic device with the integrated thermoresponsive surface at room temperature	86

LIST OF TABLES

Table 2.1: The three types of thermoresponsive surfaces fabricated with different surface roughness	12
Table 3.1: Measured temperature, time and contact angle	33
Table 5.1: Variation of the Liquid-Gas Interfacial Energy with Temperature	67
Table 5.2: Specifications of the switchable thermoresponsive valve	88

LIST OF ACRONYMS/ABBREVIATIONS

AMPD	2,2_-azobis(2-methylpropionamidine) dichloride
T_{LCS}	Absolute lower critical solution temperature of the thermoresponsive polymer
g	Acceleration due to gravity
θ_w	Apparent contact angle of a water droplet according to the Wenzel model
θ_c	Apparent contact angle of a water droplet according to the Cassie-Baxter model
ϕ_s	Area fraction according to the Cassie-Baxter model
A	Area of the microchannel cross section
AFM	Atomic force microscope
W	Average width of trapezoidal cross section of microchannel
Ca	Capillary number
L_o	Characteristic length of the liquid-gas interface
CVD	Chemical vapor deposition
θ_{sat}	Contact angle of a water droplet at T_{sat}
θ_{thr}	Contact angle of a water droplet at T_{thr}
θ_{min}	Contact angle of a water droplet on the thermoresponsive surface at room temperature
θ_{LCS}	Contact angle of the water droplet at T_{LCS}
θ_e	Contact angle of the water droplet on a flat surface
θ	Contact angle of the water droplet on the thermoresponsive surface
θ_{range}	Contact angle range between A_l and A_u
ρ	Density of water
η	Dynamic viscosity

FLBL	Flow through Layer-by-Layer
R_f	Fluidic resistance
ΔP_L	Hagen-Poiseuille (laminar flow) pressure drop
h_{H2O}	Height of the water column
h	Height/depth of microchannel
R_h	Hydraulic radius
IC	Integrated circuit
σ_{LV}	Interfacial liquid-vapor surface tension
σ_{SV}	Interfacial solid-vapor surface energy
σ_{SL}	Interfacial solid-liquid surface energy
ε	Kinematic viscosity
LOC	Lab-on-a-chip
LBL	Layer-by-layer
L	Length of the microchannel
U_d	Linear velocity of fluid flow
A_l	Lower bound of the modified logistic function
LCST	Lower critical solution temperature
β	Magnitude compensation factor
P_{max}	Maximum pressure differential that the thermoresponsive surface can withstand at a given temperature
MEMS	Micro-electro-mechanical systems
EDC	<i>N</i> -(3-dimethylaminopropyl)- <i>N</i> -ethylcarbodiimide
T	Operating temperature
P	Perimeter of the microchannel cross section
PAA	Poly(acrylic acid)
PAH	Poly(allylamine hydrochloride)
PNIPAAm	Poly(<i>N</i> -isopropylacrylamide)
PDMS	Polydimethylsiloxane
ΔP	Pressure differential

R_1, R_2	Principal radii of curvature of advancing meniscus of water
R_c	Process dependent fitting parameter of the modified logistic function
C_{slp}	Process dependent saturation slope coefficient of the modified logistic function
δ_{LCS}	Rate of temperature fall over the LCST range
Re	Reynolds number
r	Roughness factor according to the Wenzel model
φ_{sat}	Saturation slope factor
T_{sat}	Saturation temperature of the thermoresponsive polymer
SEM	Scanning electron microscope
$\theta''(T)$	Second differential of the modified logistic function
m	Slope of the modified logistic function
m_{H_2O}	Slope of the pressure sensor calibration curve
m_{time}	Slope of the time response of the thermosensitive surface
T_{thr}	Threshold temperature of the thermoresponsive polymer
k	Transition slope factor of the logistic function
t_h	Transition time of the thermoresponsive polymer to switch from hydrophobic regime to hydrophilic regime
A_u	Upper bound of the modified logistic function
Q	Volumetric flow rate
We	Weber number
ΔP_s	Young-Laplace (surface tension) pressure drop

CHAPTER 1: INTRODUCTION

1.1. Research Motivation

Micro-electro-mechanical systems (MEMS)/microelectronic/microfluidic devices and chemical/optical/biological sensors integrated with nano dimensional materials have invoked great research interest as these materials exhibit novel and enhanced properties as compared to their bulk counterparts. In addition to the advantage of a small size, devices integrated with the appropriate nanomaterials show new characteristics such as high selectivity, sensitivity, throughput, output efficiency and reduced power/reagent consumption leading to the development of cost effective devices and systems.

According to a report [1] from Business Communications Company, Inc. (BCC), a leading market research company, the estimated the global market for nanotechnology products was nearly \$9.4 billion in 2005 and over \$11.5 billion in 2007. It is estimated to increase to about \$27 billion by 2013 (a compound annual growth rate of 16.3%). The growth of the nanotechnology market is shown in Figure 1.1.

One of the challenging aspects in the deployment of a device/system containing nanostructures is the efficient *integration of the nanostructures into the device*.

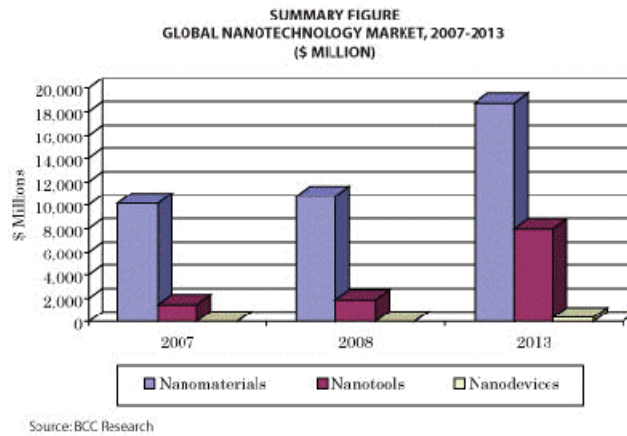


Figure 1.1: Global Nanotechnology Market, 2005-2013 [1]

Since the invention of the transistor at Bell Lab in 1947, the semiconductor industry has achieved tremendous success in mass production of integrated circuits (IC) via planar batch processing [2]. The standard semiconductor IC fabrication technology has been adapted, modified and further developed for the fabrication of MEMS and microfluidic systems [3].

Out of recent progress in chemistry and materials science, a wide variety of sub 10 nm-scale engineering materials in wire, tube or particle form have been created [4-6]. On the other side, lithographic techniques generate micrometer scale feature in reliable manners [7-11]. Interface of those two needs to be explored for successful implementation of

nanomaterial into working devices and systems [12]. The process of design and fabrication of a nanostructure integrated device can be broadly classified into three steps: selection of proper materials, integration of the nanostructures into the device and/or self assembly and finally developing a full scale product from the conceptual device. Therefore integration of nanostructures is the vital link between the material selection and the final product.

1.2. Previous Work and Research Objectives

Surfaces that can tune their properties when subjected to external stimuli have potential applications in a variety of fields including drug delivery [13], bioanalysis [14], protein separation [15] and microfluidics [16]. Surfaces which change their wettability with varying temperature have drawn considerable attention as their hydrophobicity can be finely tuned over a wide range of stimuli. These surfaces have a variety of applications including microflow regulation [17], force transduction [18], drug delivery [19] and molecular filtering [20]. One of the primary objectives of this work is to develop an analytical model for the wettability switching characteristic of a unique nanostructured thermoresponsive surface synthesized from the polymer PNIPAAm. PNIPAAm is a well known polymer that is sensitive to changes in the ambient heat and has a lower critical solution temperature (LCST) range of about 28–33 °C. The polymer chains hydrate and stay in extended structures when the solution temperature is below the LCST range, giving rise to hydrophilic structures. In contrast, the polymer chains form intramolecular

hydrogen bonds and dehydrate when the solution temperature increases above the LCST range, resulting in compact hydrophobic structures [21]. PNIPAAm can be grafted on a rough surface to create surface that can switch from superhydrophobicity to superhydrophilicity by varying the ambient temperature [22]. An analytical model is required in order to understand and implement this switching behavior into useful applications. An exhaustive mathematical analysis of this unique thermosensitive phenomenon is pursued in this work. The switching characteristic of the PNIPAAm surface is modeled on a modified logistic function. Logistic functions to describe various phenomenon have been reported [23, 24].

The second objective is to develop a smart surface that utilizes the wettability control integrating the thermoresponsive polymer and a microheater. The temperature rise for the switching of the thermoresponsive surface can be provided by metallic microheaters. Metallic microheaters have been used as a heat source in various applications including cell culture [25] and cell immobilization [26]. Temperature modulated PNIPAAm surfaces have been used as platforms for attachment/detachment of endothelial cells and hepatocytes [27]. In this work, the PNIPAAm surface is heated by spiral gold microheaters which are fabricated on the lower side of the glass substrate. The contact angle change with change in temperature is tested using a standard goniometer. Detailed time response analysis of the surface and the gain of the PNIPAAm have been experimentally determined and also verified theoretically.

The switchable thermosensitive surface can be efficiently integrated into microfluidic systems for flow regulation based on the fluid-structure interaction effects. Passive microfluidic valves based on abrupt geometric transition [28], incorporation of hydrophobic material in the microchannel [29], fluid flow rectifying nozzles [30] and diffusers [31], Tesla elements [32] have been investigated. All these valves have a non-tunable functionality and cannot switch from hydrophilicity to hydrophobicity. Some tunable surfaces based on electrowetting have been reported, but these require high actuation voltage, have limited tunability and a complex fabrication process [33, 34]. A unique microfluidic regulator which can switch its surface characteristic from hydrophilic to hydrophobic in response to ambient temperature change, hence achieving regulation of fluid flow due to fluid- surface interaction, is the third study objective of this research. The PNIPAAm thermosensitive regulator has low power requirements and a wide range of contact angle tunability. The polymers are deposited by using the LBL deposition technique. Polyelectrolyte multilayers assembled by LBL technique have been extensively studied over the past decade and show promise in numerous applications [35, 36]. In the current work, two fully integrated proof-of-concept microfluidic valves, one with a superhydrophobic polymer surface and the other with a switchable, thermosensitive polymer surface have been fabricated and tested [17]. The passive valve with the superhydrophobic polymer surface selectively inhibits the flow of water-based reagents and passes aqueous solutions containing surfactants. In case of the thermosensitive valve, the switchable polymer surface becomes hydrophobic when heated to temperatures exceeding 65 °C, thus inhibiting the flow of water and becomes hydrophilic at room temperature, thus allowing the flow of water. The microchannels are

fabricated by standard photolithography and wet etching techniques. The polymer surface for both the valves is fabricated using the LBL deposition technique, in which multiple layers of polyelectrolytes are coated on a channel wall followed by silica nanoparticle treatment. For the thermosensitive valve, the polymer surface is further coated with the thermosensitive polymer poly(*N* isopropylacrylamide) (PNIPAAm). The fabricated microfluidic valve was tested with liquids flowing in the microchannels under capillary action. It is shown that the valve selectively regulates the flow of test samples.

For seamless large scale integration of the thermosensitive switchable microfluidic valve into an LOC system, the critical operating specifications of the valve are to be understood. The final objective is to characterize the thermoresponsive microfluidic regulator in terms of the pressure differential between the inlet and outlet. Straight microfluidic channels with various geometries were fabricated and the thermosensitive polymer was selectively coated inside the channel. A differential transducer was connected to the valve and pressure measurement was performed using standard data logging set up. The development of pressure head and differential pressure inside thick capillaries has been well established by numerous classical fluid mechanics theories [37-40]. The hydraulic radius of the microchannel is used in the Hagen-Poiseuille equation to calculate the pressure drop to establish laminar flow. Assuming a constant advancing contact angle, the principle radii of curvature of the fluid are used in the Young-Laplace equation to calculate the pressure drop to overcome the surface tension across the advancing meniscus. Summation of the Hagen-Poiseuille pressure drop and the Young-

Laplace drop results in the total pressure drop. The important characteristic parameters such as capillary, Weber and Reynolds numbers in association with operating conditions will be discussed on theoretical and experimental basis.

CHAPTER 2: ANALYTICAL MODEL FOR THE WETTABILITY SWITCHING CHARACTERISTICS OF NANOSTRUCTURED THERMORESPONSIVE SURFACES

Conventionally, the equilibrium contact angle of a water droplet on a flat surface (θ_e) in relation to the surface energies can be expressed by the Young's equation [41] as:

$$\cos(\theta_e) = \frac{\sigma_{SV} - \sigma_{SL}}{\sigma_{LV}} \quad (2.1)$$

where σ_{SV} , σ_{SL} and σ_{LV} are the interfacial surface energies between the solid-vapor, solid-liquid and liquid-vapor phases respectively.

The hydrophobicity of a surface depends on its surface energy and roughness. The energy of a surface is determined by the surface functional groups. The effect of roughness on hydrophobicity is described by the Wenzel model [42] and the Cassie model [43].

2.1. Modeling Contact Angle of Rough Surfaces

The Wenzel model can be used in the hydrophilic regime ($\theta_e < 90^\circ$) and hydrophobic regime ($90^\circ < \theta_e < 150^\circ$) while the Cassie model can be used in the superhydrophobic regime ($\theta_e > 150^\circ$) [44].

2.1.1. Wenzel Model

In the Wenzel theory, it is assumed that the water drop fills the grooves of the rough surface and hence forms a wetted contact. The apparent contact angle of the water droplet on a rough surface according to the Wenzel model (θ_w) can be expressed as:

$$\cos(\theta_w) = r \cos(\theta_e) \quad (2.2)$$

where r is the roughness factor and is defined as the ratio of the actual surface to the geometric surface.

2.1.2. Cassie-Baxter Model

In the Cassie-Baxter theory, it is assumed that the water droplet does not fill the grooves of a rough surface and forms a composite contact [45].

The apparent contact angle of a water droplet on a rough surface according to the Cassie model (θ_c) can be expressed as:

$$\cos(\theta_c) = \phi_s [\cos(\theta_e) + 1] - 1 \quad (2.3)$$

where ϕ_s is area fraction of the liquid-solid contact and represents the surface roughness.

These models explain the influence of surface roughness in the amplification of the surface wetting characteristics. The contact angle of a water droplet on a hydrophobic surface can be increased by incorporating high surface roughness and low surface energy.

2.2. Synthesis of Superhydrophobic Surfaces

Based on the Wenzel and Cassie-Baxter models, a multilayered polyelectrolyte surface decorated with silica nanoparticles and functionalized with a low surface energy material could be fabricated to realize superhydrophobic surface [46].

In the current work, first, a micro-nano structured (polyelectrolyte-silica nanoparticle) base was created, followed by grafting the thermoresponsive polymer (PNIPAAm) and finally a low surface energy material (perfluorosilane) was deposited to realize a unique surface with variable wettability. Using this approach, the hydrophobicity of the surface could be considerably increased.

Layer-by-Layer (LBL) deposition technique was used to build uniform and conformal multilayer films of poly(allylamine hydrochloride) (PAH) and silica nanoparticles with a precise control of film thickness and roughness. The porous polyelectrolyte multilayers

give rise to roughness on the micron scale and the silica nanoparticles give roughness at the nano scale. The surface was further functionalized with PNIPAAm. As a result, the PNIPAAm molecules make the surface switchable between hydrophobic and hydrophilic in response to the temperature variation. Three different kinds of thermoresponsive surfaces, fabricated on glass slides for studying the switching characteristics are described in Table 2.1.

Table 2.1: The three types of thermoresponsive surfaces fabricated with different surface roughness

<p>Surface A</p> <p>Intermediate surface roughness</p>	<p>Surface with a polyelectrolyte-silica nanoparticle base, on to which a very thin layer of PNIPAAm is grafted, such that the PNIPAAm is present only on the surface and does not fill the pores of the base. The PNIPAAm layer does not cover the surface completely and the nanoscale surface roughness is retained. This is shown in Atomic Force Microscope (AFM) image of Figure 2.1 (a), where we can still see the shape of the individual nanoparticles.</p>
<p>Surface B</p> <p>Low surface roughness</p>	<p>Surface with a polyelectrolyte-silica nanoparticle base, on to which a very thick layer of PNIPAAm is grafted, such that the PNIPAAm is present on the surface and also fills up the pores of the base. The PNIPAAm layer covers the surface completely and the nanoscale roughness is eliminated as shown in Figure 2.1 (b).</p>
<p>Surface C</p> <p>High surface roughness</p>	<p>Surface similar to surface (B), but in this case the surface roughness is regenerated by depositing a very thin layer of silica nanoparticles on the PNIPAAm surface. The switching action due to the PNIPAAm is still retained as the silica nanoparticles do not cover the surface completely. This is shown in Figure 2.1 (c).</p>

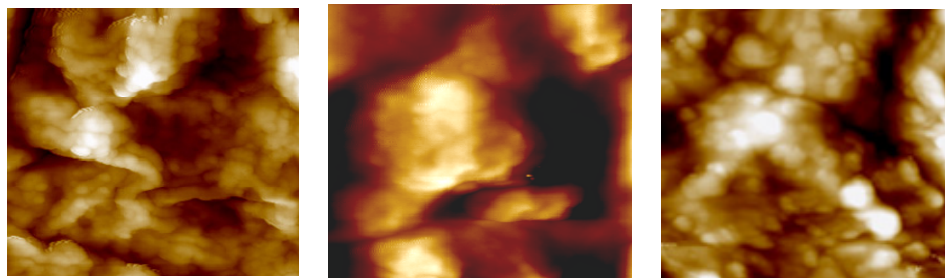


Figure 2.1: AFM height images of (a) A very thin layer of PNIPAAm deposited on rough multilayer film (Surface A). (b) A thick layer of PNIPAAm deposition after 2 hours polymerization which reduces roughness (Surface B). (c) Nanoscale roughness is reintroduced with silica nanoparticle deposition on the thick PNIPAAm polymer film (Surface C). (The size of all images is 1micron).

Atomic Force Microscopy (AFM) height and phase images were collected using an AFM microscope (Pico SPM) in tapping mode. AFM images were obtained with scan sizes ranging from 500 nm to 1 μm . All images were obtained using tapping mode imaging with a single silicon probe (Force constant of 0.5-9.5 N/m). The scan angle was maintained at 0° , and the images were captured in the trace direction with a scan rate of 56-58 KHz.

Surface C was finally functionalized with a very thin layer of a low surface energy material, (1H, 1H, 2H, 2H-perfluorooctyl) silane (perfluorosilane). The combination of surface roughness and chemical composition created a switchable superhydrophobic/hydrophilic surface. X-ray Photoelectron Spectroscopy (XPS) analysis was carried out for all the samples to determine the surface composition.

2.3. Switching Characteristics of the Thermoresponsive Surfaces

The tuning of hydrophobicity was quantified by measuring the change in the contact angle of a water droplet placed on the surface of the sample as the temperature of the surface was varied. The contact angle was measured using a standard goniometer (Ramehart Inc.). The surface temperature was varied using a flexible DC heater (Omega Engineering Inc.). A K-type, chromium-aluminum, fine gauge thermocouple (Omega Engineering Inc.) was attached to the surface to measure the temperature variation.

The switching characteristics depicting the variation of contact angle versus temperature are shown in Figure 2.2 (a-c) for each type of surface. Surface C shows a higher maximum and minimum contact angle than surface B at the maximum and minimum operating temperatures respectively. This is due to the inherent higher average surface roughness of surface C.

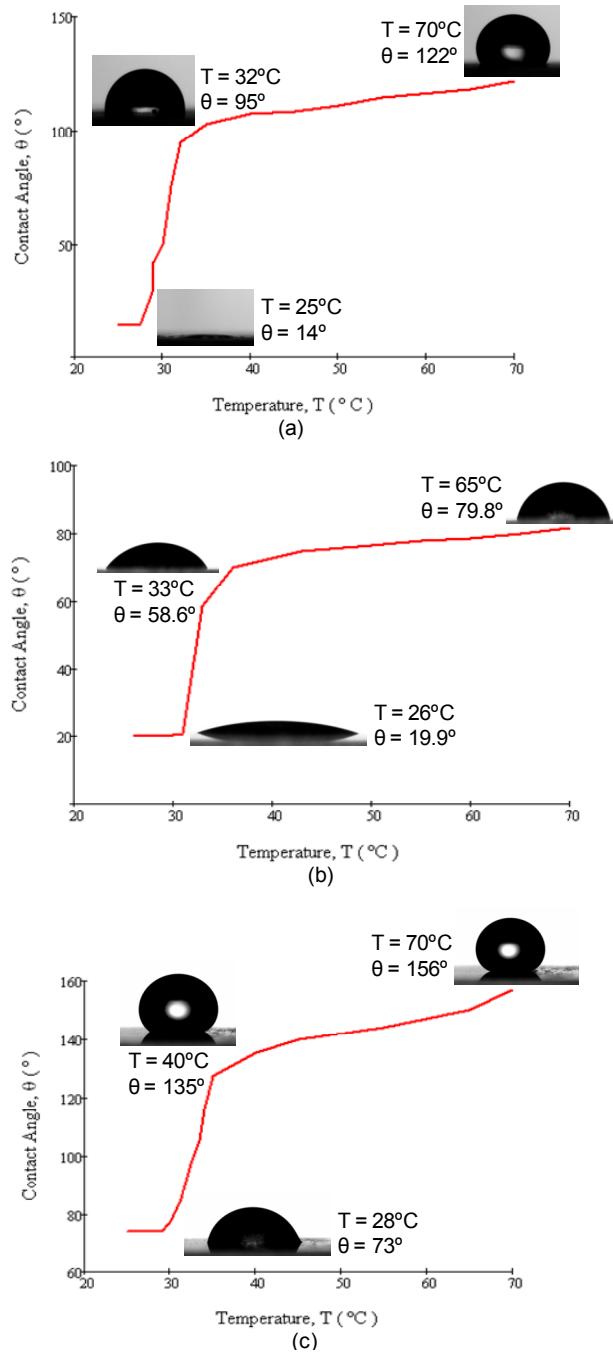


Figure 2.2: (a) Plot of contact angle versus surface temperature for surface A. Inset: Optical micrographs of the water droplet at low, medium and high temperatures. (b) Plot of contact angle versus surface temperature for surface B. Inset: Optical micrographs of the water droplet at low, medium and high temperatures. (c) Plot of contact angle versus surface temperature for surface C. Inset: Optical micrographs of the water droplet at low, medium and high temperatures.

2.4. Analytical Model for the Switching Characteristic of the Thermoresponsive Surface

An analytical model for the switching characteristic of a thermoresponsive surface is very useful for predicting the contact angle of a water droplet on the switchable surface and for developing other important material characteristics of the surface.

The switching characteristic can be modeled on a standard logistic function, which is expressed by the general equation:

$$Y(x) = \frac{1}{1+e^{-kx}} \quad (2.4)$$

where k is the transition slope factor of the function.

Starting from Eq. 2.4, a modified logistic function was developed to fit the ordinate & abscissa values, transition & saturation slope, surface roughness and the LCST of the polymer.

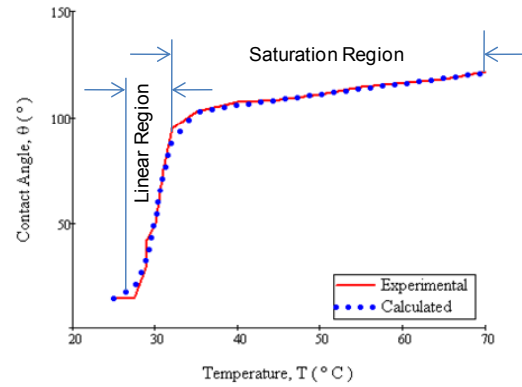
The equation for the contact angle of a water droplet (θ) can be given by:

$$\theta(T) = \theta_{min} + \frac{\beta + \varphi_{sat}}{1+e^{-k(T-T_{LCS})}} \quad (2.5)$$

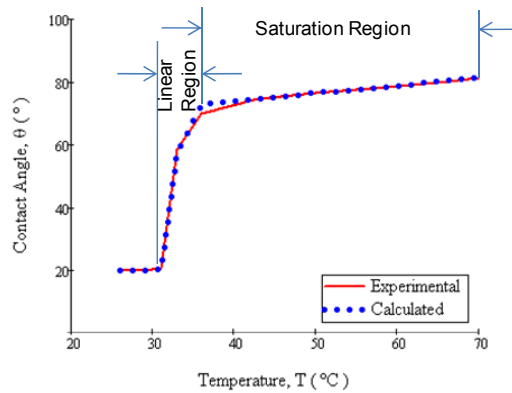
where, T is the operating temperature, θ_{min} is the contact angle at room temperature, β is the magnitude compensation factor, φ_{sat} is the saturation slope factor and T_{LCS} is the

absolute lower critical solution temperature of the thermosensitive polymer. The curve given by Equation (2.5) can be divided into two regions, namely, the linear and the saturation region. The linear region spans the LCST range and exhibits maximum gain. The magnitude compensation can be characterized by $\beta = \frac{\theta_{max}}{R_c}$, where θ_{max} is the contact angle at maximum operating temperature and R_c is a process dependent fitting parameter. As the temperature is increased beyond the linear region, the gain in hydrophobicity becomes minimal and gives rise to the slope in the saturation region. The saturation slope factor can be defined as $\varphi_{sat}(T) = \frac{T}{C_{slp}}$, where C_{slp} is a process dependent saturation slope coefficient.

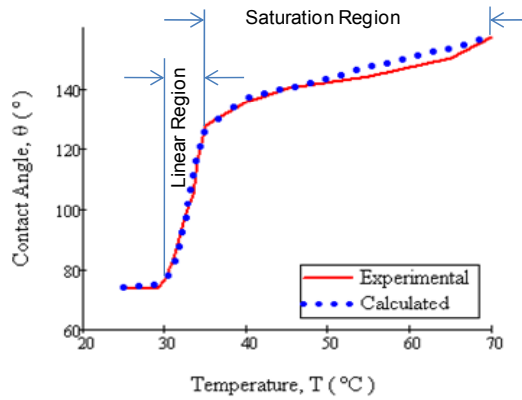
In the saturation region, the water droplet is subjected to competing forces. The droplet absorbs heat energy of the test sample on which it is placed, resulting in a decrease of the surface energy of the water droplet. On the other hand, the hydrophobic nature of the thermosensitive polymer and the roughness of the sample tend to increase the surface energy of the water droplet. Figure 2.3 (a), (b) and (c) shows the theoretical curve fitted on to the experimental curve of surfaces A, B and C respectively.



Process Parameters: $R_c = 1.68$; $C_{slp} = 2$; $k = 1$; $T_{LCS} \approx 30.25^\circ\text{C}$
 (a)



Process Parameters: $R_c = 1.85$; $C_{slp} = 4$; $k = 3$; $T_{LCS} \approx 32.7^\circ\text{C}$
 (b)



Process Parameters: $R_c = 4.32$; $C_{slp} = 1.5$; $k = 1$; $T_{LCS} \approx 33^\circ\text{C}$
 (c)

Figure 2.3: (a) Plot of the calculated contact angle fitted on the measured contact angle versus surface temperature for surface A. (b) Plot of the calculated contact angle fitted on the measured contact angle versus surface temperature for surface B. (c) Plot of the calculated contact angle fitted on the measured contact angle versus surface temperature for surface C.

The T_{LCS} of the polymer occurs at approximately the midpoint of the transition slope. “Surface B” shows faster switching due to a thicker layer of PNIPAAm, manifested in the transfer characteristic equation as a higher value of k . The value of C_{slp} is inversely proportional to the saturation slope. Hence, a lower value of C_{slp} is required to model “Surface C”. We use the switching characteristic of Surface A for further mathematical analysis. The first and second differentials of Equation (2.5) are given by:

$$m = \frac{e^{k(T-T_{LCS})} + k(T + \beta C_{slp}) + 1}{4 C_{slp} \cosh\left[\frac{k(T-T_{LCS})}{2}\right]^2} \quad (2.6)$$

$$\theta''(T) = \frac{k e^{k(T_{LCS}-T)} [(2+T k + \beta k C_{slp}) e^{k(T_{LCS}-T)} - k(T + \beta C_{slp}) + 2]}{C_{slp} (e^{k(T_{LCS}-T)} + 1)^3} \quad (2.7)$$

Figure 2.4 shows the plot of the slope and second differential of the contact angle versus temperature. We can clearly see that the relative local maxima occurs approximately at the T_{LCS} i.e. at the point where θ'' crosses the zero of the ordinate axis. The maximum gain (i.e. the maximum value of m) of the contact angle also occurs at the T_{LCS} .

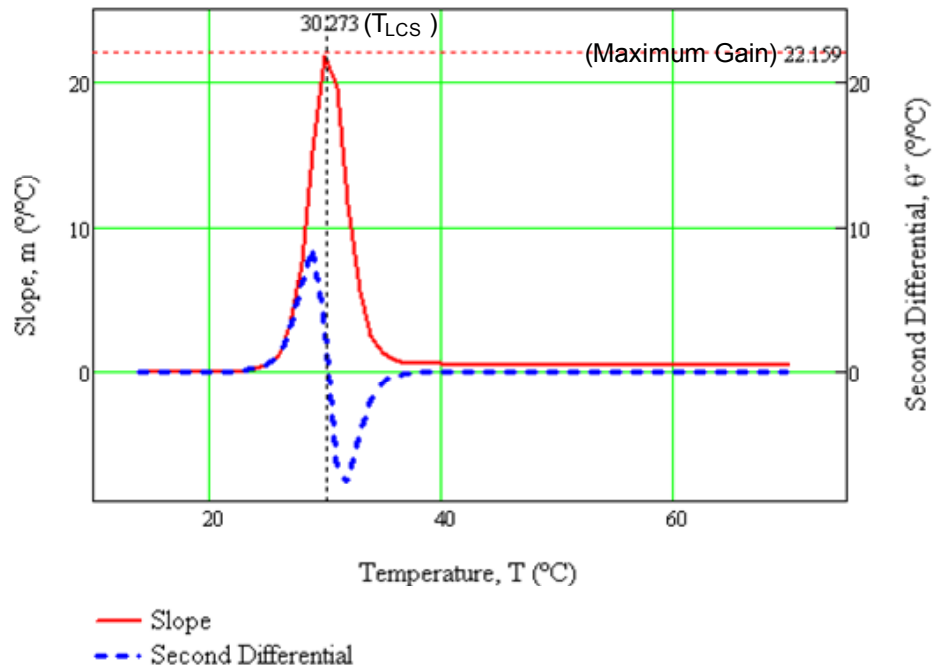


Figure 2.4: Plot of the first and second differential of the contact angle versus the surface temperature for surface A.

The defining metric of a thermoresponsive polymer is the onset and end temperatures of the LCST range. These temperatures can be calculated by using the piece-wise linear approximation approach. The linear region of the transfer function given by Equation (2.5) can be represented by a straight line which intersects an upper (A_u) and a lower ($A_l = \theta_{min}$) bound.

The boundaries are defined over a contact angle range ($\theta_{range} = A_u - A_l$), such that $\theta_{LCS} = \theta_{min} + \frac{\theta_{range}}{2}$ as shown in Figure 2.5. θ_{LCS} is the contact angle of the water droplet at T_{LCS} . The onset of the LCST range, characterized by the threshold temperature T_{thr} and the end of the LCST range, characterized by the saturation temperature (T_{sat}), correspond to the points where the straight line intersects with the lower and upper bounds respectively. T_{thr} and T_{sat} are the temperatures at which the value of the contact angles are approximately 10 % above and below A_l and A_u respectively.

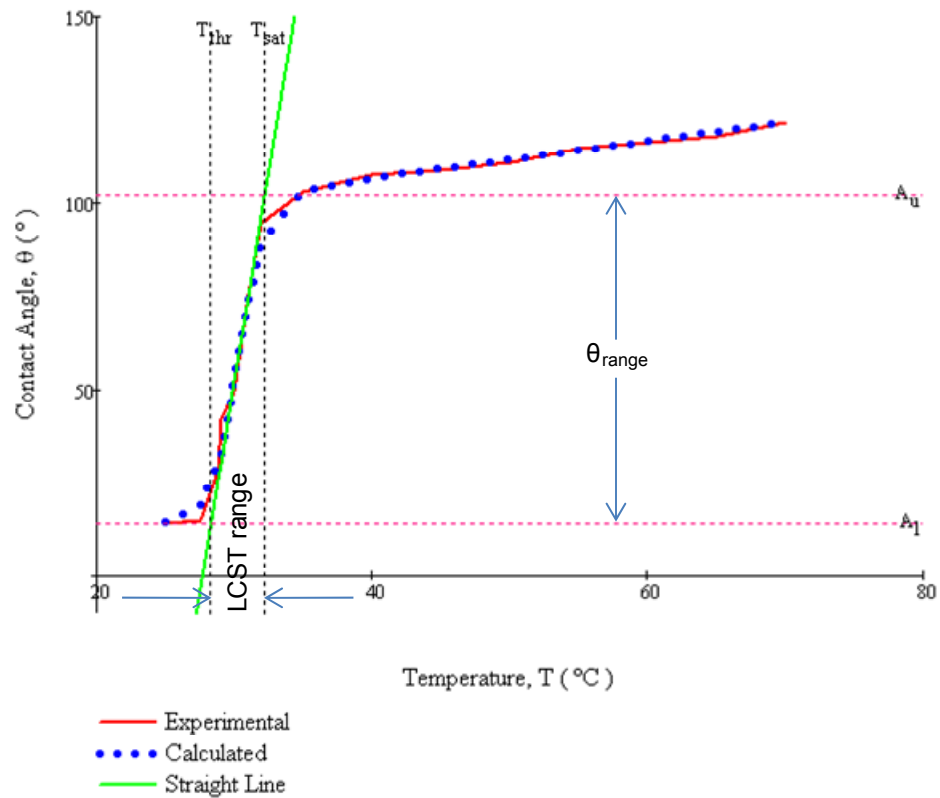


Figure 2.5: Piece-wise linear approximation method to find the threshold ($T_{thr}=28.27$ °C) and saturation ($T_{sat}= 32.23$ °C) temperatures to characterize the onset and end of the LCST range. The contact angle at T_{thr} is $\theta_{thr} = 24.73^\circ$ and at T_{sat} is $\theta_{sat} = 92.04^\circ$.

Substituting the value of m at T_{LCS} (from Equation (2.6)) and the value of the constant C (for the condition $y = \theta_{min} + \frac{\theta_{range}}{2}$ at $x = T_{LCS}$) in to the equation of the straight line $y = mx + C$, we derive an expression for the linear region of the transfer function as:

$$\theta(T) = \frac{2+k(T_{LCS}+\beta C_{stp})}{4 C_{stp}} T + \theta_{min} + \frac{\theta_{range}}{2} - \frac{T_{LCS} [k(T_{LCS}+\beta C_{stp})+2]}{4 C_{stp}} \quad (2.8)$$

Solving for the value of T_{thr} at $\theta = A_l$, we get:

$$T_{thr} = T_{LCS} - \frac{2 C_{stp} \theta_{range}}{T_{LCS} k + \beta k C_{stp} + 2} \quad (2.9)$$

Similarly, the value of T_{sat} at $\theta = A_u$ is:

$$T_{sat} = T_{LCS} + \frac{2 C_{stp} \theta_{range}}{T_{LCS} k + \beta k C_{stp} + 2} \quad (2.10)$$

By introducing the rigorous mathematical model, the characteristics of the thermoresponsive polymer could be precisely defined and identified as discussed in this chapter.

CHAPTER 3: THERMOSENSITIVE SMART SURFACE WITH INTEGRATED MICROHEATER FOR WETTABILITY CONTROL

A Multilayer polyelectrolyte surface decorated with silica nanoparticles to provide roughness and functionalized with a low surface energy material was deposited on a glass substrate. PNIPAAm was grafted on the aforementioned surface to create a tunable hydrophobic/hydrophilic smart surface for wettability control. The heating of the PNIPAAm above its LCST can be achieved by integrated metallic microheaters. Microheaters have been used for providing localized heating in a number of applications including automated microfluidic cell culture [25] and cell immobilization [26]. The thermoresponsive smart surface deposited on a glass substrate can be effectively heated using integrated metal microheaters. This device is suitable for large scale integration into Lab-on-a-chip (LOC) systems for potential applications such as automated microfluidic cell culture systems for attachment and detachment of various cell types including endothelial cells and hepatocytes [27].

3.1. Design and Fabrication

Spiral thin film structures with variable pitch are ideal as microheaters because they exhibit minimum center to edge temperature deviation [47]. Gold can be optimally used as the microheater metal as it has a linear temperature coefficient of resistance, a very

low resistivity and is inert / compatible in many biological processes. The designed gold film microheater with a variable pitch is shown in Figure 3.1.

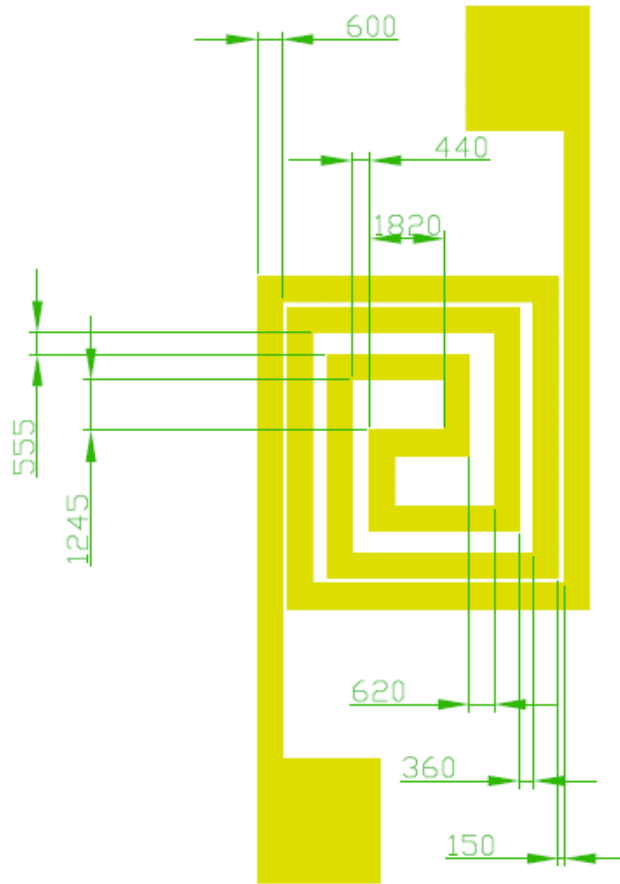


Figure 3.1: Schematic showing the dimensions of the gold thin film microheater.

The microheaters were fabricated on a glass substrate using standard photolithography and wet etching techniques [48] [49] as shown in Figure 3.2 (a-b). After coating photoresist on the microheaters for protection, the glass surface on the flip side of the

substrate was deposited with polyelectrolytes using the LBL (layer-by-layer) self assembly technique. An automated LBL coater Stratosequence VI (Nanostrata Inc.) was used to deposit 43 bilayers of poly(allylamine hydrochloride) (PAH) and silica nanoparticles on the glass substrate as shown in Figure 3.2 (c). The pH of the polyelectrolyte and silica nanoparticle solution was chosen to obtain an optimum degree of ionization to generate a rough surface with appropriate thickness [50].

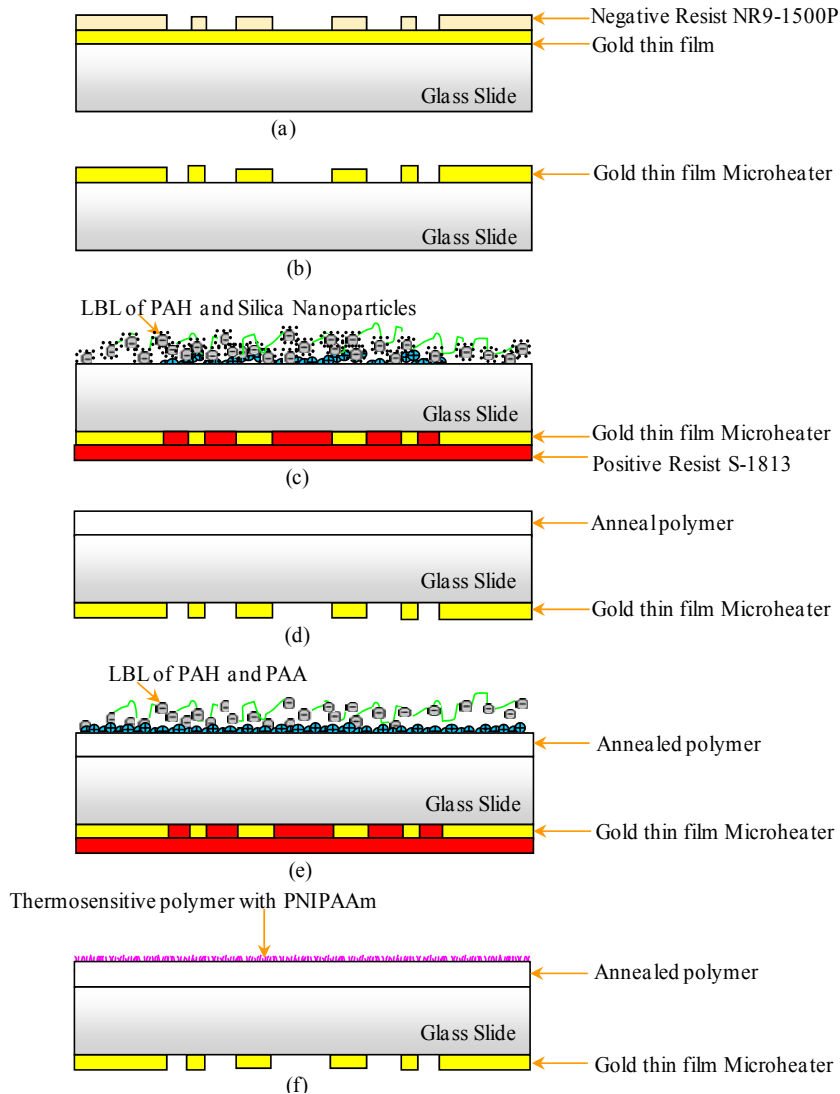


Figure 3.2: Fabrication process for the Thermosensitive Polymer-on-Microheater smart platform. (a) Gold thin film deposited on a glass slide is lithographically patterned. (b) Gold is wet etched to form the microheater structure. (c) The microheater is protected by coating photoresist and the flip side of the glass substrate is deposited with polyelectrolytes. Positively charged poly(allylamine hydrochloride) (PAH) followed by negatively charged silica nanoparticles are dip coated by LBL deposition till 80 layers of PAH and silica nanoparticles are deposited. (d) The glass platform with the rough polymer surface is annealed at 400 °C for 2 hours, (e) Again, with the microheater protected with photoresist, 4 layers of PAH and poly(acrylic acid) (PAA) are deposited by LBL method followed by free-radical initiator deposition. (f) Poly(N-isopropylacrylamide) (PNIPAAm) is grafted to create the switchable, thermosensitive polymer surface.

The metal lines of the microheater structure have inherent roughness which tends to affect the wettability of the surface. The thermoresponsive switchable polymer was created on the bare glass surface on the flip side of the substrate to ensure that the observed hydrophobicity of a water droplet is solely due to action of the smart surface and not due to the roughness of the metallic microheaters. The heat generated by the microheaters which are on the lower side of a glass substrate, is easily transmitted to the thermosensitive surface on the upper side of the substrate.

The multilayered, porous polymer was weakly attached to the glass surface by forces created by opposing charges. Hence the surface is made robust and adaptable for further processing by annealing the glass substrate at 400 °C for 2 hours as shown in Figure 3.2 (d).

On the top of multilayered coating, two bilayers of PAH and poly(acrylic acid) (PAA) were deposited with PAA as the last layer followed by free radical initiator coupling for the subsequent grafting of thermosensitive polymer PNIPAAm as shown in Figure 3.2 (e). Thermosensitive PNIPAAm was grafted on initiator modified multilayer films according to a reported approach [51] as shown in Figure 3.2 (f). Finally perfluorosilane which is a low surface energy material was deposited on the polymer

surface by chemical vapor deposition (CVD) to increase the hydrophobicity of the thermosensitive polymer surface.

3.2. Results and Discussion

An AFM image of the fabricated polymer smart surface is shown in Figure 3.3 (a). The fabricated platform is shown in Figure 3.3 (b).

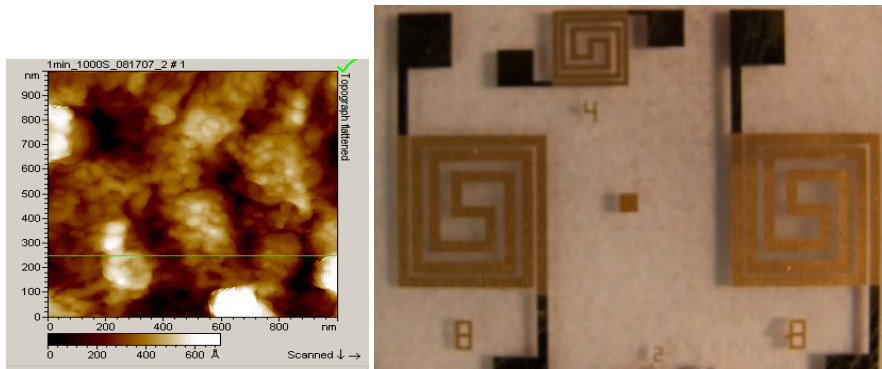


Figure 3.3: (a) AFM image of the thermosensitive polymer PNIPAAm decorated with silica nanoparticles to enhance the surface roughness. A very thin layer of PNIPAAm is optimum to achieve the highest hydrophobicity. (b) Fabricated Switchable Thermosensitive Polymer-on-Microheater platform.

The smart polymer surface on the upper side of the glass substrate is heated by the integrated microheater on the lower side. The microheater is connected to a variable DC power supply and the temperature of the PNIPAAm surface is monitored using a standard

chromium-aluminum K-type fine gauge thermocouple (Omega Engineering Inc.). The temperature variation is repeatable and reliable for characterizing the thermosensitive platform. Surface wettability tuning is quantified by measuring the contact angle of a water droplet on the thermoresponsive surface using a standard goniometer (Ramehart Inc.). Initially the thermoresponsive surface is heated up to an elevated temperature and a water droplet is placed on the surface. The contact angle of the water drop decreases as the surface is allowed to cool down gradually by step wise decrement of the applied voltage to the microheater. Contact angle of the water drop on the platform ranges from 18° at room temperature to 125° at approximately 70 °C.

3.3. Time Response Analysis

Figure 3.4 shows the plot of the variation of the contact angle of the water droplet and the temperature of the thermoresponsive surface versus applied voltage to the microheater.

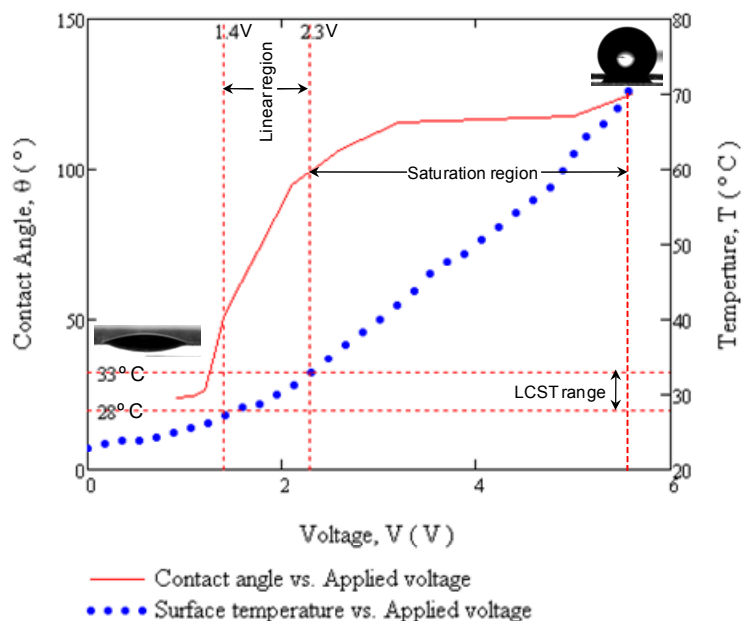


Figure 3.4: Plot of variation of the contact angle of a water droplet and variation of temperature of the smart thermoresponsive surface versus voltage applied to the microheater (Inset: Hydrophobic and Hydrophilic drop on the thermoresponsive polymer platform).

It can be observed that the temperature of the smart surface linearly varies with the voltage applied to the microheater over the entire operating temperature range from 22 °C to 90 °C. The contact angle of the surface varies rapidly over the LCST range while the variation is much slower at elevated or around room temperatures. Accordingly the plot can be divided into the linear range and the saturation range. The shape of the contact angle plot can be modeled by a modified sigmoidal logistic function as discussed in CHAPTER 2.

An important metric of the smart surface is the time response. The time response is crucial to study the hydrophobic/hydrophilic switchability of the surface for the development of fluid regulating devices. The decrease in the contact angle of the water drop on the thermoresponsive platform with the decrease in the surface temperature was recorded at fixed intervals of time to quantify the time response. The plot of the contact angle change with time is shown in Figure 3.5.

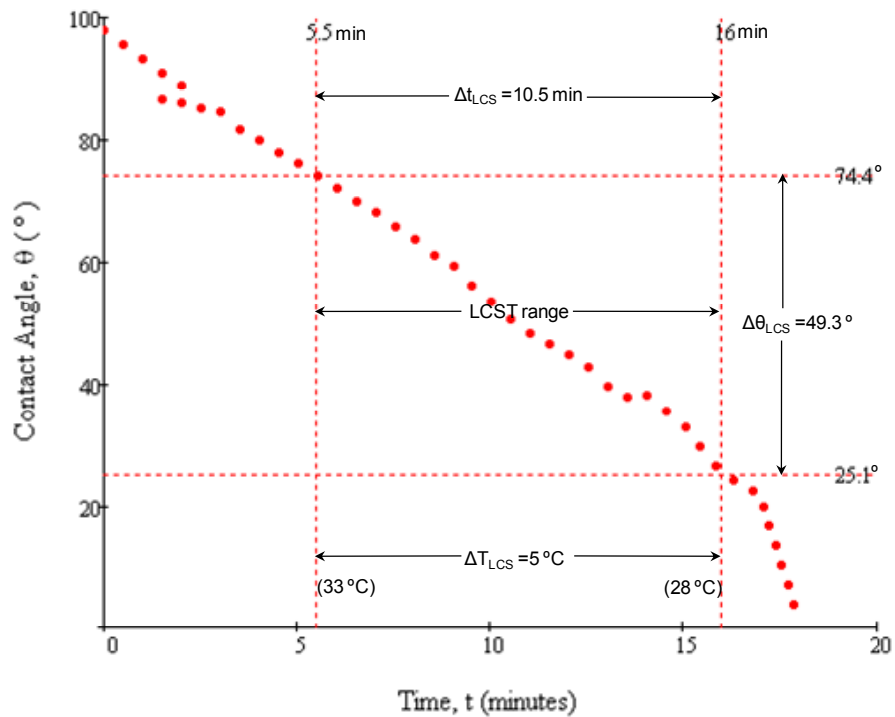


Figure 3.5: Plot of contact angle change of a water droplet on the thermosensitive surface versus time.

We define the temperature, time and contact angle difference over the LCST range as $\Delta T_{LCST} = (33 - 28) \text{ }^\circ\text{C}$, $\Delta t_{LCST} = (16 - 5.5) \text{ min}$ and $\Delta \theta_{LCST} = (74.4 - 25.1)^\circ$ respectively. The approximate slope of the line in the LCST range (28 °C to 33 °C) is:

$$m_{time} = \Delta \theta_{LCST} / \Delta t_{LCST} = -4.695 \text{ }^\circ / \text{min} \quad (3.1)$$

This value indicates the reduction rate of contact angle upon cooling.

With the current set up of the metallic microheaters, the rate of temperature fall over the LCST range is:

$$\delta_{LCST} = \Delta T_{LCST} / \Delta t_{LCST} = 0.476 \text{ }^\circ\text{C} / \text{min} \quad (3.2)$$

Considering the contact angle of 90° to be the starting of the hydrophobic regime, the switch from hydrophobicity to hydrophilicity can be calculated as the time required for the smart surface to transition from a contact angle of 100° to 80°. This transition time is given by:

$$t_h = (100 - 80)^\circ\text{C} / m = 4.26 \text{ min} \quad (3.3)$$

Obviously the time t_h will be much lower if the rate of temperature fall / rise (δ_{LCST}) is made higher.

Table 3.1 gives the values of the measured contact angles and corresponding time and temperature over a range of 49 °C to 27 °C. The difference between successive readings is also shown.

Table 3.1: Measured temperature, time and contact angle.

Temperature, T (°C)	Time, t (minutes)	Contact angle, θ (°)
T ₁ = 49	t ₁ = 0	$\theta_1=98.1$
T ₂ = 43 ($\Delta T_1 = T_2 - T_1 = 6$)	t ₂ = 1 ($\Delta t_1 = t_2 - t_1 = 1$)	$\theta_2=93.3$ ($\Delta\theta_1=\theta_2-\theta_1=4.8$)
T ₃ = 41 ($\Delta T_2 = T_3 - T_2 = 2$)	t ₃ = 1.5 ($\Delta t_2 = t_3 - t_2 = 0.5$)	$\theta_3=91.1$ ($\Delta\theta_2=\theta_3-\theta_2=2.2$)
T ₄ = 39 ($\Delta T_3 = 2$)	t ₄ = 2 ($\Delta t_3 = 0.5$)	$\theta_4=88.9$ ($\Delta\theta_3=2.2$)
T ₅ = 38 ($\Delta T_4 = 1$)	t ₅ = 2.5 ($\Delta t_4 = 0.5$)	$\theta_5=86.5$ ($\Delta\theta_4=2.4$)
T ₆ = 37 ($\Delta T_5 = 1$)	t ₆ = 3 ($\Delta t_5 = 0.5$)	$\theta_6=84.6$ ($\Delta\theta_5=1.9$)
T ₇ = 36 ($\Delta T_6 = 1$)	t ₇ = 3.5 ($\Delta t_6 = 0.5$)	$\theta_7=82.1$ ($\Delta\theta_6=2.5$)
T ₈ = 35 ($\Delta T_7 = 1$)	t ₈ = 4 ($\Delta t_7 = 0.5$)	$\theta_8=80.2$ ($\Delta\theta_7=1.9$)
T ₉ = 34 ($\Delta T_8 = 1$)	t ₉ = 4.5 ($\Delta t_8 = 0.5$)	$\theta_9=78.3$ ($\Delta\theta_8=1.9$)
T ₁₀ = 33 ($\Delta T_9 = 1$)	t ₁₀ = 5.5 ($\Delta t_9 = 1$)	$\theta_{10}=74.4$ ($\Delta\theta_9=3.9$)
T ₁₁ = 32 ($\Delta T_{10} = 1$)	t ₁₁ = 6.5 ($\Delta t_{10} = 1$)	$\theta_{11}=70$ ($\Delta\theta_{10}=4.4$)
T ₁₂ = 31 ($\Delta T_{11} = 1$)	t ₁₂ = 7.5 ($\Delta t_{11} = 1$)	$\theta_{12}=66.1$ ($\Delta\theta_{11}=3.9$)
T ₁₃ = 30 ($\Delta T_{12} = 1$)	t ₁₃ = 9.5 ($\Delta t_{12} = 2$)	$\theta_{13}=56.1$ ($\Delta\theta_{12}=10$)
T ₁₄ = 29 ($\Delta T_{13} = 1$)	t ₁₄ = 12 ($\Delta t_{13} = 2.5$)	$\theta_{14}=45.2$ ($\Delta\theta_{13}=10.9$)
T ₁₅ = 28 ($\Delta T_{14} = 1$)	t ₁₅ = 16 ($\Delta t_{14} = 4$)	$\theta_{15}=25.1$ ($\Delta\theta_{14}=20.1$)
T ₁₆ = 27 ($\Delta T_{15} = 1$)	t ₁₆ = 20 ($\Delta t_{15} = 4$)	$\theta_{16} = 18$ ($\Delta\theta_{15}=7.1$)

To visualize the contact angle gain in the LCST range, it is useful to define a differential normalized contact angle $\Delta\theta/\Delta T$, as the change in contact angle per unit change in temperature. The contact angle tuning of the water droplet on the smart surface is a function of temperature. Hence the time response of the contact angle variation is also

related to the temperature. The normalized contact angle will reflect the time response incorporating the temperature dependence.

Using Table 3.1 the normalized contact angle versus the total time over the entire temperature range is plotted as shown in Figure 3.6. The largest normalized gain is 3.05°C-min and occurs between 30°C (7.5 minute) and 31°C (9.5 minute). The average normalized contact angle gain over the LCST range of $28^{\circ}\text{C} - 33^{\circ}\text{C}$ is $1.543^{\circ}\text{C-min}$. As shown in Figure 3.6, the gain before and after the LCST range is much lower than that in the LCST range.

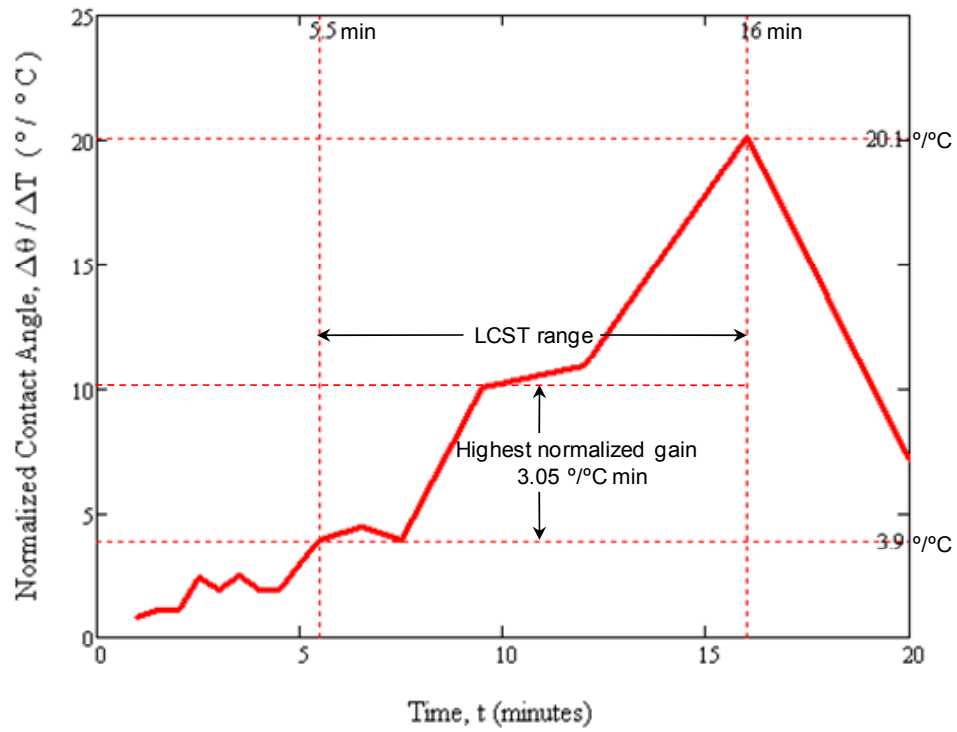


Figure 3.6: Time response of the thermoresponsive smart surface. Plot shows normalized contact angle variation versus time.

CHAPTER 4: MICROFLUIDIC FLOW REGULATION BASED ON SUPERHYDROPHOBIC NANOSTRUCTURES AND SWITCHABLE THERMOSENSITIVE SURFACE

The field of microfluidics is in a nascent stage of development and there is tremendous research emphasis on developing basic microfluidic devices like pumps and valves based on various phenomena [52]. The development of micropumps and microvalves has made it possible to realize a fully integrated microfluidic system for biochemical analysis [28, 53, 54]. Previously developed flow regulation techniques for microfluidic devices are dependent on the pH of the solution flowing in the microchannels [55]. Nano/microliter fluid handling on LOC by passive fluidic manipulation often employs a hydrophobic surface as a valve in the microchannel network and an external pneumatic control coupled with capillary action to discretely manipulate the fluids. Capillary manipulation of fluids by modifying the solid–liquid surface tension, using surfaces with wettability gradients have been shown to be well adapted for microfluidic systems [56].

Wettability of a solid surface is an important property of a material as it controls its interaction with the liquid. It depends on various factors, among which surface roughness and surface energy are the dominant ones. For the fabrication of superhydrophobic surface, a combination of optimum surface roughness and low surface energy is required. Wenzel's model proposed that the roughness increases the surface area which geometrically increases the hydrophobicity [42]. In fact, surfaces with a water contact

angle of more than 150° were fabricated by incorporating appropriate roughness on materials having low surface energies.

By extending these studies, we propose novel microfluidic valves, in which the microchannel network is selectively coated with functionalized polymers, using the LBL deposition technique. Two different microfluidic valves based on different gating mechanisms were chosen as proof of concept devices:

- (a) A passive microfluidic valve with an integrated superhydrophobic surface to control the flow of reagent based on the surface energy of the sample fluid.
- (b) A thermosensitive microfluidic valve with an integrated switchable thermosensitive, hydrophobic/hydrophilic surface to control the flow of reagent based on the temperature of the polymer surface.

In the LBL technique the degree of ionization of weak polyelectrolytes is dependent on their pH. By controlling the pH of weak polyelectrolytes, the molecular structure and properties of resulting multilayer films can be precisely tuned. This pH dependency is exploited in the deposition technique to create very thin polyelectrolyte layers [50].

It has been reported that aqueous solutions of various surfactants can wet a superhydrophobic surface, as the surfactant reduces the surface tension of the solution [57]. The polymer in our valve is superhydrophobic to water-based reagents which have high surface tension (surface tension of water is 72.2 mJ/m^2) but is wettable by an organic-based solvent like 2-propanol which has low surface tension (surface tension of 2-propanol is 21.7 mJ/m^2). This achieves valving action by selectively inhibiting the flow of water while passing 2-isopropanol.

The selectively coated thermosensitive polymer in our valve exhibits hydrophobicity when heated to temperatures above $65 \text{ }^\circ\text{C}$ and hydrophilicity at room temperature for all water-based reagents having high surface tension. This achieves gating of the sample reagents based on the temperature of the switchable polymer surface.

The polyelectrolytes in the multilayered film, fabricated by LBL, are held by weak ionic bonds. Hence the polymer cannot withstand any vigorous microfabrication processes that use strong acids or bases. These limiting factors make the integration of the LBL polymers significantly challenging.

The overall process has been developed such that the polymer surface can be created with minimum number of LBL depositions and a robust polymer surface which is compatible with most of the standard microfabrication processes is obtained with reduced processing steps and time.

4.1. Design

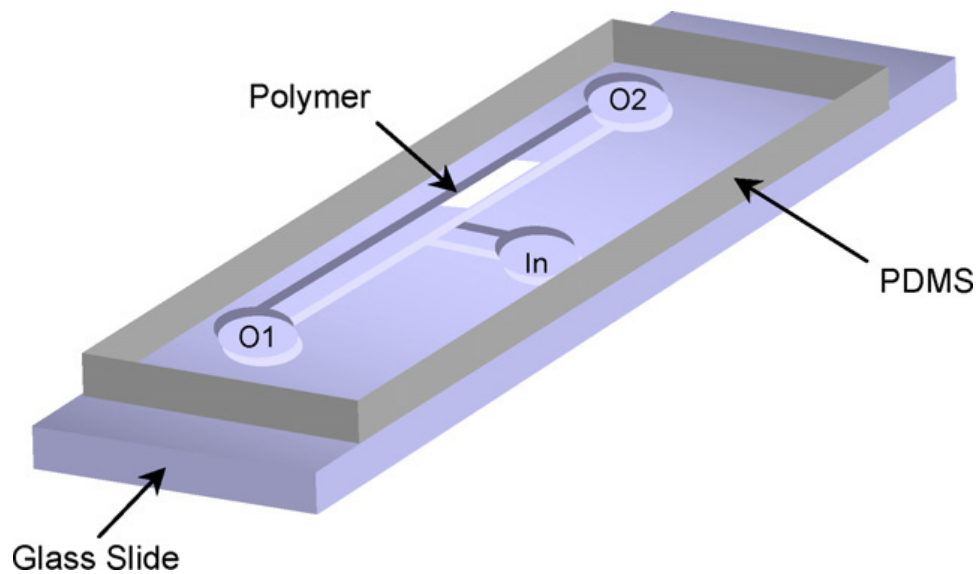


Figure 4.1: Schematic of the flow regulator. In-Inlet; O1-Outlet 1; O2-Outlet 2.

Figure 4.1 shows a schematic illustration of the device. The same design has been used to demonstrate the working concept of both types of microfluidic valves. A simple T-

junction microfluidic channel structure that connects one inlet and two outlets was chosen. A polymer patch in one branch of the channel is used as the valve to gate the incoming flow depending on the surface tension characteristics or the temperature.

4.2. Fabrication of the Passive Microfluidic Valve with the Superhydrophobic Surface

4.2.1. Microchannel Fabrication

Figure 4.1 shows the fabrication process flow for the valve. The bare borosilicate glass slides are initially prepared by the RCA standard cleaning. The detailed procedure for RCA cleaning is described in APPENDIX A. A positive photoresist, AZ-4903 (AZ Electronic Materials USA Corp.) is then spin-coated to a thickness of approximately 20 μm . The photoresist is patterned by UV photolithography to define the T-junction microchannel structure (Figure 4.2 (a)). The glass etch solution consists of 0.8% (v/v) hydrofluoric acid and 32% (v/v) sulfuric acid [58]. The etchant has an etch rate of approximately 0.35 $\mu\text{m}/\text{min}$ and the etching is carried out at 30 °C. The glass was etched to create channels of around 50 μm depth (Figure 4.2 (b)). This etch produces a linear profile and a smooth etched surface. The detailed procedure for RCA cleaning is described in APPENDIX B. This etching technique requires only the photoresist (AZ 4903) as the etching mask and eliminates the need for metal etching masks.

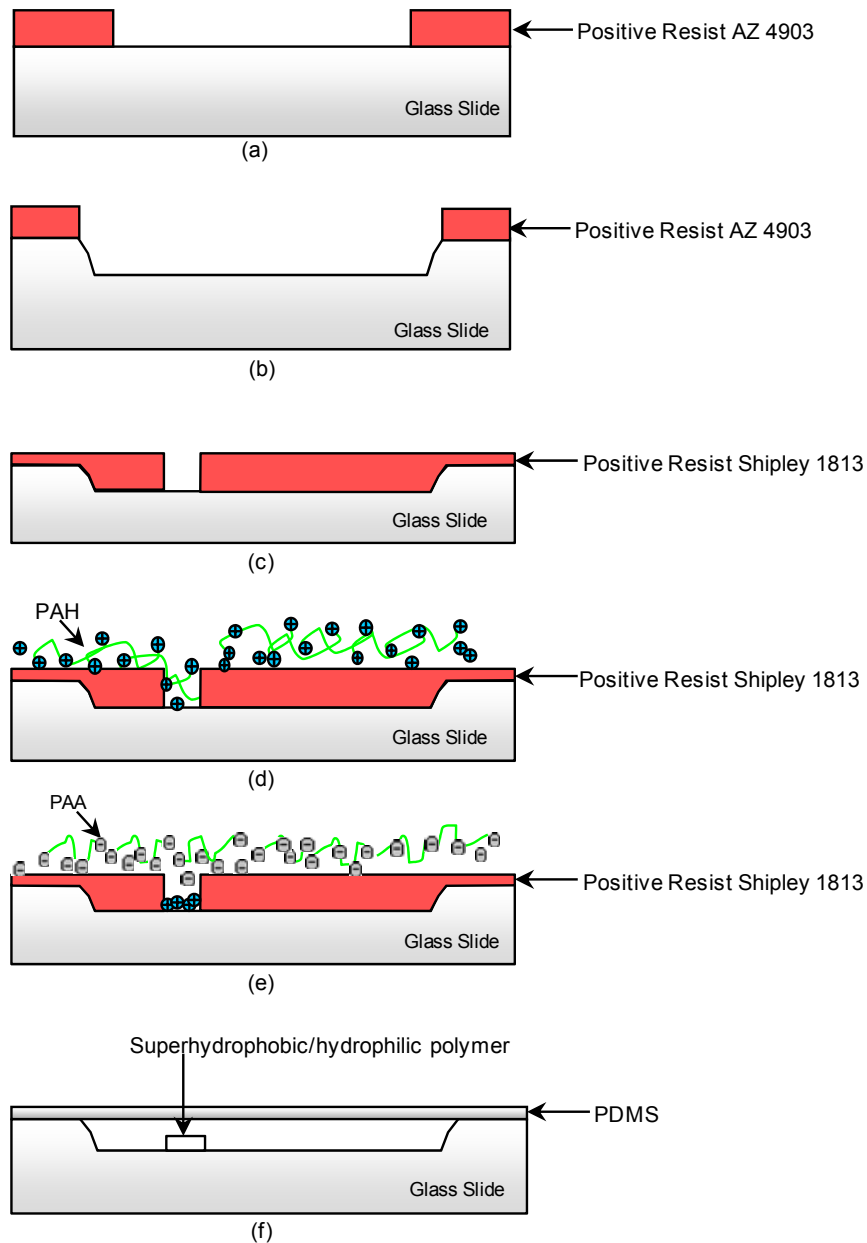


Figure 4.2: Fabrication process the passive valve. (a) Glass slide is lithographically patterned to form the T-junction microchannel. (b) The patterned glass slide is wet etched by using the photoresist as an etch mask. (c) The glass slide is photolithographically patterned to form an opening for the initial polyelectrolytes. (d) Positively charged poly(allylamine hydrochloride) (PAH) is dip coated on the opening. (e) Negatively charged poly(acrylic acid)(PAA) is then dip coated. This LBL deposition is continued successively till 101 bilayers of PAH and PAA are formed. (f) A Polydimethylsiloxane (PDMS) slab is bonded to the glass slide after oxygen plasma treatment.

4.2.2. Polyelectrolyte Deposition

A positive photoresist Microposit S1813 (Shipley Company) is spin-coated on the etched glass slide and patterned photolithographically to produce openings for the initial polyelectrolytes deposition as shown in Figure 4.2 (c). The polyelectrolyte patch is deposited using the LBL self-assembling technique. An automated LBL coater Stratosequence VI (Nanostrata Inc.) is used to deposit 101 bilayers of poly(allylamine hydrochloride) (PAH) and poly(acrylic acid) (PAA) on the patterned glass substrate, with the outermost layer being PAH as shown in Figure 4.2 (d) and (e). The pH of PAH and PAA is maintained at 8.5 and 3.5 respectively. The pH is chosen to get an optimum degree of ionization to generate a rough coating with appropriate thickness after subsequent acidic treatment [46, 50]. The surface of the multilayer film is roughened by immersing the glass slides, first, in an acidic solution at pH 2.7 for 2 h and then in a solution at pH 2.3 for 4 h (pH was adjusted with 0.05 M HCl). The film is crosslinked by baking the glass slide for 2 hours at 180 °C.

4.2.3. Polydimethylsiloxane (PDMS) Bonding and Interconnection

A fully cured PDMS slab can be irreversibly bonded to a glass slide after both the surfaces are exposed to oxygen plasma and immediately brought into contact with each other. The irreversible bonding is due to the formation of bridging covalent siloxane (Si–O–Si) bonds between the PDMS and glass surfaces [59]. PDMS elastomer (Sylgard 184, Dow Corning) and curing agent were mixed with a ratio of 10:1 (by weight) and cured at

100 °C for 45 min. A 17-gauge blunt reusable steel needle was used to core through holes in the PDMS for the inlet and outlets. The cured PDMS slab and the glass slide with the etched microchannels (containing the selectively coated roughened polyelectrolyte film) are subjected to oxygen plasma activation in a reactive ion etcher (Plasmalab RIE), then immediately brought into contact with each other to form a leak proof seal as shown in Figure 4.2 (f). A moderate RF power of 70 W, an oxygen pressure of 100 mTorr and a very short treatment time were found to produce the best results for this kind of bonding [60]. Polymer tubings were inserted into the holes.

4.2.4. Fabrication of the Superhydrophobic surface

To create nanoscale features on the roughened polyelectrolyte surface, a 0.01 M solution of PAH followed by a 0.028% (w/v) silica nanoparticle solution (Ludox TM 40, Aldrich: 40 wt% silica nanoparticle suspension in water, particle size ~22 nm) was introduced successively through the microchannels using a syringe pump. The silica nanoparticles are negatively charged. Since the roughened polyelectrolyte surface is coated with a layer of positively charged PAH, the silica nanoparticles attach to the rough surface. Taking into account the very small particle size of TM 40 (~22 nm) compared to the dimension of the channel and the fact that only one bilayer is deposited, we can assume that this deposition does not interfere with the flow of fluid through the channel, although there is some attachment of PAH and silica nanoparticles on the glass channel.

To create a superhydrophobic surface, a network of long chain (1H,1H,2H,2H-perfluorooctyl) silane molecules were coated on the patch, by pumping into the microchannels, 0.6% (w/v) perfluorosilane dissolved in isopropyl alcohol. The perfluorosilane molecules reduce the surface energy [61, 62] of the polymer surface. Finally the sample is baked at 90 °C overnight.

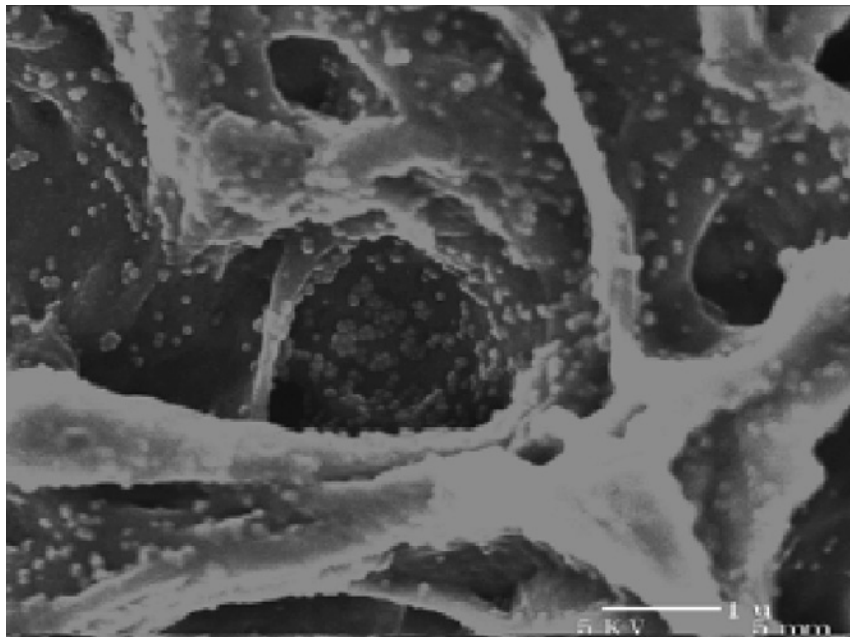


Figure 4.3: Silica nanoparticles on porous multilayered polyelectrolyte surface - (scale bar = 1 μm).

Figure 4.3 shows the SEM image of the silica nanoparticles coated on the roughened polyelectrolyte surface.

4.3. Fabrication of the Microfluidic Valve with the Thermosensitive Polymer

4.3.1. Initial Polyelectrolyte Deposition

T-junction microchannel structure is etched in a glass slide and openings are photolithographically patterned on the device for initial polymer deposition as described in 4.2.1 and 4.2.2. An automated LBL coater is used to dip coat 40 bilayers of PAH and silica nanoparticles on the patterned glass substrate as shown in Figure 4.4 (a) and (b). The pH of PAH solution and silica nanoparticle solution is maintained at 7.5 and 9.0, respectively. The silica solution consists of 0.069% (w/v) (Ludox SM 30, Aldrich, particle size ~7 nm) and 0.081% (w/v) (Ludox TM 40, Aldrich, particle size ~20 nm) nanoparticle suspensions in 0.1 M NaCl solution. The concentration of the nanoparticle solution is adjusted to 0.1 M to aid the formation of thick layers of silica nanoparticles. This step creates a rough, multilayered, porous silica/polymer surface.

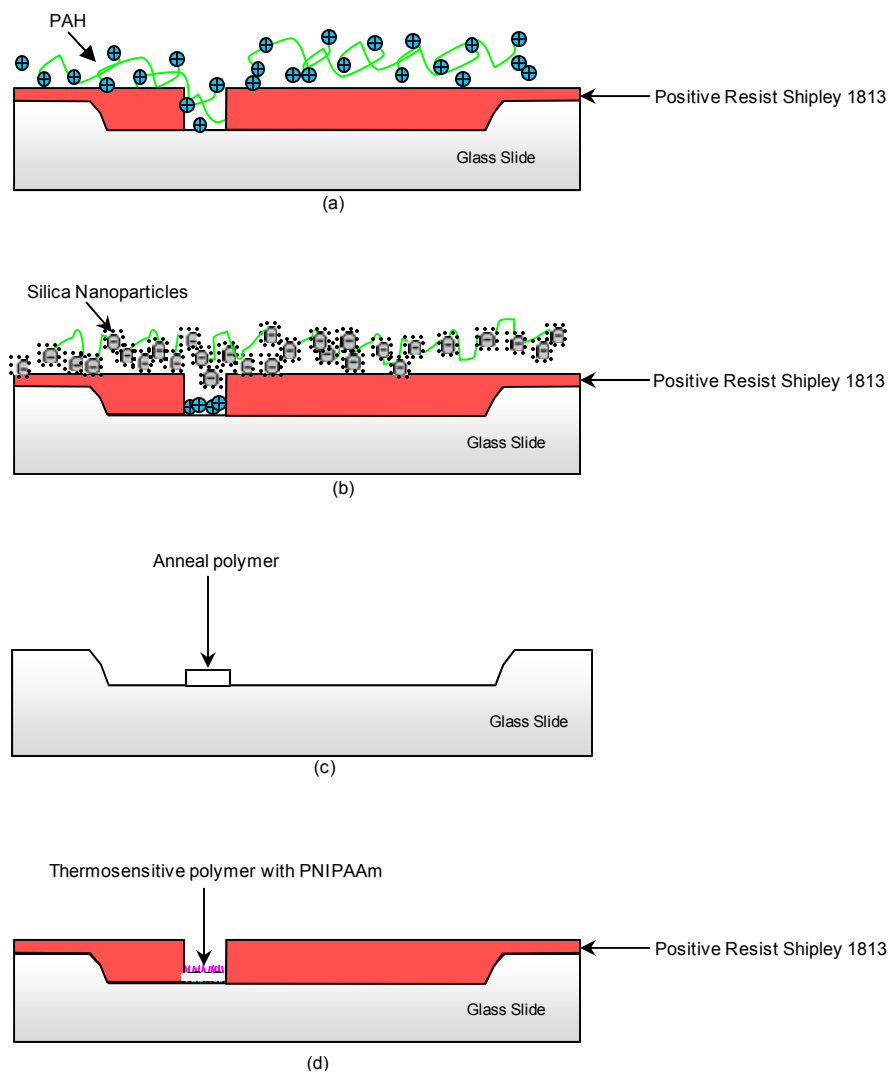


Figure 4.4: Fabrication process for the thermosensitive valve. (a) The etched glass slide with a lithographically patterned opening for the initial polyelectrolytes is dip-coated with positively charged poly(allylamine hydrochloride) (PAH). (b) Negatively charged silica nanoparticles are then dip-coated. This LBL deposition is continued successively till 40 bilayers of PAH and silica nanoparticles are formed. This is followed by a second run of LBL deposition to decorate the polymer surface with silica nanoparticles. (c) The glass chip with the rough polymer surface is annealed at 400 °C for 2 h. (d) After a third run of LBL deposition to create two bilayers of PAH and PAA, the glass chip is dipped into the initiator solution for 2 h. Finally PNIPAAm is grafted onto the initiator-coated surface to create the switchable, thermosensitive polymer surface.

4.3.2. Annealing

The multilayered polymer surface is weakly attached to the glass platform by forces created by opposing charges. Hence the surface is not adaptable for further processing and needs to be made robust. This is achieved by annealing the microfluidic glass chip with the integrated polymer surface, at 400 °C for 2 h as shown in Figure 4.4 (c). This fuses the silica nanoparticles into the glass, makes the patch robust and also increases the roughness further.

4.3.3. Initiator Deposition

On the top of crosslinked porous coating, two bilayers of PAH (pH 8.5) and PAA (pH 3.5) were deposited with PAA as the last layer. The negatively charged PAA provides carboxylate groups to attach the initiators for the subsequent grafting of thermosensitive polymers. The initiator solution consists of 1 g of 2,2'-azobis(2-methylpropionamide) dichloride (AMPD) and 0.494 g of *N*-(3-dimethylaminopropyl)-*N*-ethylcarbodiimide (EDC, the catalyst) dissolved in 100 ml of water. The valve with the PAA functionalized polymer patch is placed into the aqueous solution of the free-radical initiator and allowed to react for 2 h. This creates an initiator layer on the rough and porous polymer patch onto which the thermosensitive polymer PNIPAAm can be grafted. The initiator-derivatized sample is rinsed in deionized water, dried, and used immediately for polymerization.

4.3.4. Thermosensitive Polymer (PNIPAAm) and Perfluorosilane Deposition

Thermosensitive PNIPAAm was grafted on initiator modified multilayer films according to a reported approach [51]. Recrystallized NIPAAm is dissolved in deionized water at 1% (w/v). The initiator-modified glass sample is immersed into this solution, and the whole solution is purged with nitrogen gas for 15 min to remove the dissolved oxygen. Then, 0.135 g of AMPD is added quickly and the reaction vessel is sealed immediately. It is placed in a preheated oil bath. Polymerization reaction is carried out typically at 65 °C which is indicated by the milky white appearance of the reaction solution. The sample is removed from the reaction vessel as soon as the solution turned milky to ensure a very thin layer of polymer formation on the patch. The sample is washed in deionized water and dried.

The thermal tunability of the valve depends on the PNIPAAm polymerization time. We have found that a very short period of polymerization reaction is the most optimum as it deposits a very thin layer of polymer (PNIPAAm) on the rough multilayer surface, which maintain the surface roughness required for hydrophobicity. On the other hand, polymerization carried out for long time generates a very thick layer of PNIPAAm which fills up all the pores and reduces surface roughness. Thus the short-time polymerization process on the rough surface renders the polymer surface hydrophobic and at the same time makes it thermally switchable.

The subsequent chemical vapor deposition (CVD) of (1H,1H,2H,2H-perfluorooctyl) silane on the polymer patch increase the hydrophobicity of the thermosensitive polymer surface.

Finally the photoresist on the glass chip is stripped off and the device is baked overnight at 140 °C. PDMS is bonded on the device to form a leak proof seal as described in 4.2.3.

4.4. Test Results and Discussion

Figure 4.5 shows the final fabricated device on a glass substrate. Figure 4.6 shows the SEM micrograph of the cross-section of etched glass channel sealed with a leak proof flat PDMS slab.

The final thickness of the selectively deposited gating polymer in both types of valves is approximately 5 μm as shown in Figure 4.7. The cross-section of the thermosensitive polymer deposited on the glass channel was observed using SEM. We believe that the superhydrophobic polymer in the passive valve has a thickness in the same range due to the similarity in the processing conditions.

For the valve test, a programmable syringe pump (Harvard PHD 2000) was used to pump dye-colored water at 20 $\mu\text{l/h}$ into the inlet reservoir and then the liquid was allowed to flow in the microchannels under capillary action only.

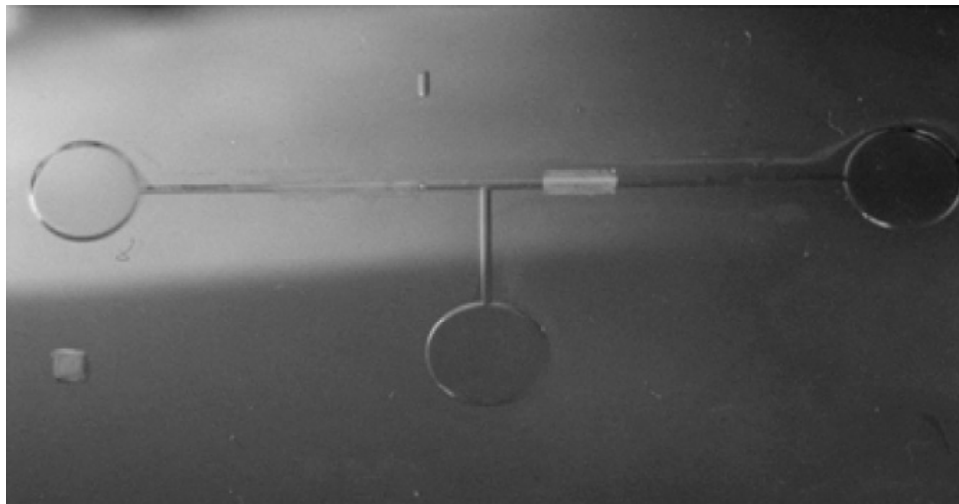


Figure 4.5: Fabricated structure showing the inlet/outlet reservoirs and the superhydrophobic/hydrophilic polymer film (shown as white patch in the right microchannel).

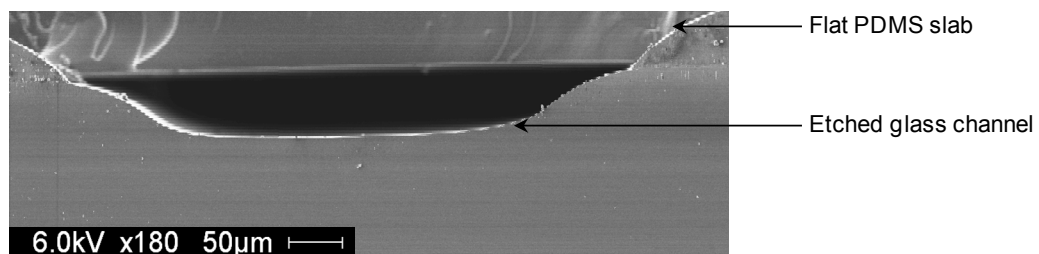


Figure 4.6: SEM micrograph of the cross-section of the etched glass channel with a PDMS seal.

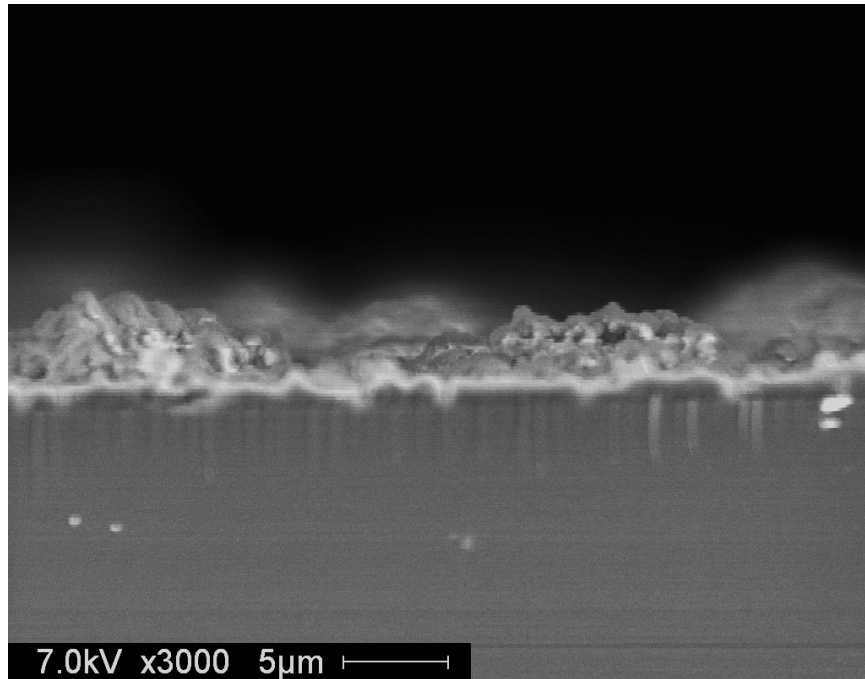


Figure 4.7: SEM micrograph of switchable thermoresponsive polymer deposited inside etched glass capillary.

4.4.1. Passive Microfluidic Valve with Superhydrophobic Surface

Figure 4.8 shows the change in the contact angle of water/2-propanol drop on a superhydrophobic surface with varying 2-isopropanol concentration. Increasing concentration of 2-propanol decreases the surface tension of the solution and hence produces lower contact angles [63].

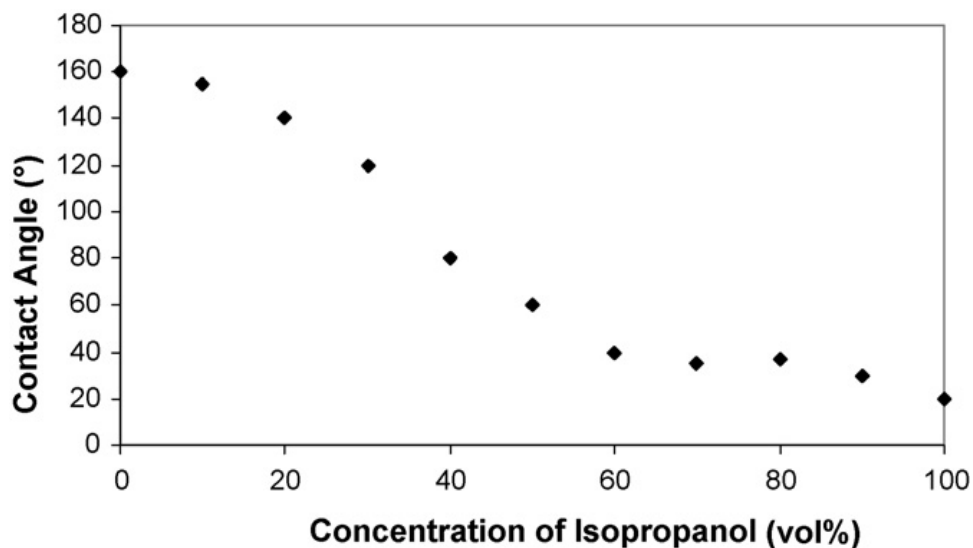


Figure 4.8: Contact angle vs. concentration of water/2-isopropanol mixtures on a polymer surface.

The “closed” status of the valve is observed when the water stops at the film interface because of the superhydrophobic polymer film surface (Figure 4.9). When 2-isopropanol solution flows in the microchannels under capillary action, the polymer film is readily wetted due to reduced surface tension between the surfactant solution and the polymer surface. The 2-isopropanol solution passes over the polymer film resulting in “open” action of the valve as shown in Figure 4.10 (a) and (b).

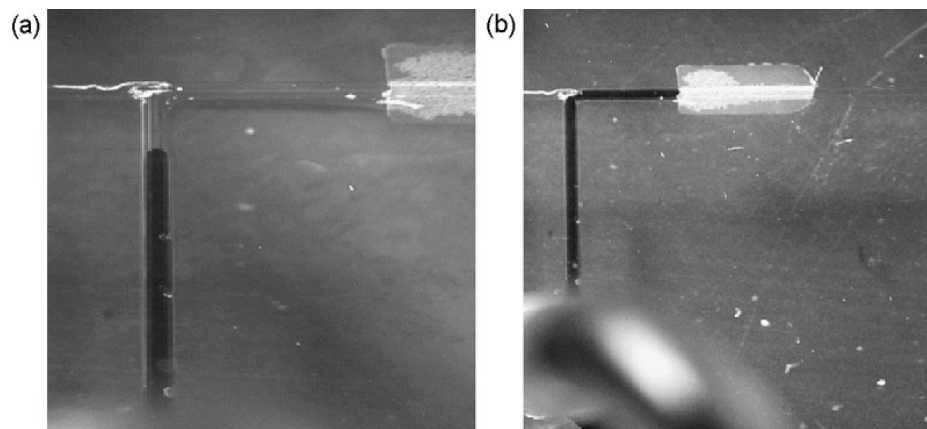


Figure 4.9: "Closed" status of the valve: (a) dyed water approaches junction and (b) water is stopped at the superhydrophobic polymer surface.

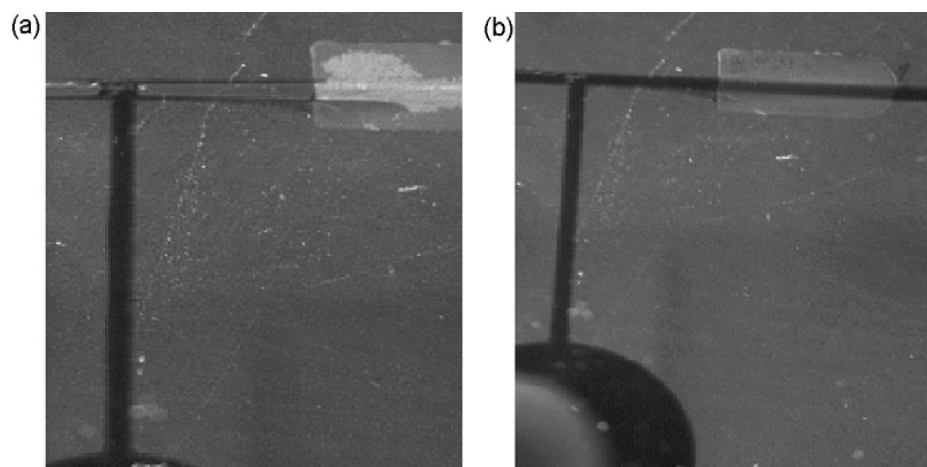


Figure 4.10: "Open" status of the valve: (a) 2-isopropanol approaches junction and (b) 2-isopropanol wets the polymer surface and flows over it.

4.4.2. Microfluidic Valve with the Thermosensitive Polymer

As mentioned before, PNIPAAm forms intramolecular hydrogen bonds above its LCST and becomes hydrophobic. Therefore, it is expected that the wetting properties of the rough surface grafted with PNIPAAm will switch from hydrophobic to hydrophilic when the ambient temperature decreases. Figure 4.11 shows the plot of contact angle versus temperature. It is clear that the contact angle decreases dramatically at PNIPAAm's LCST.

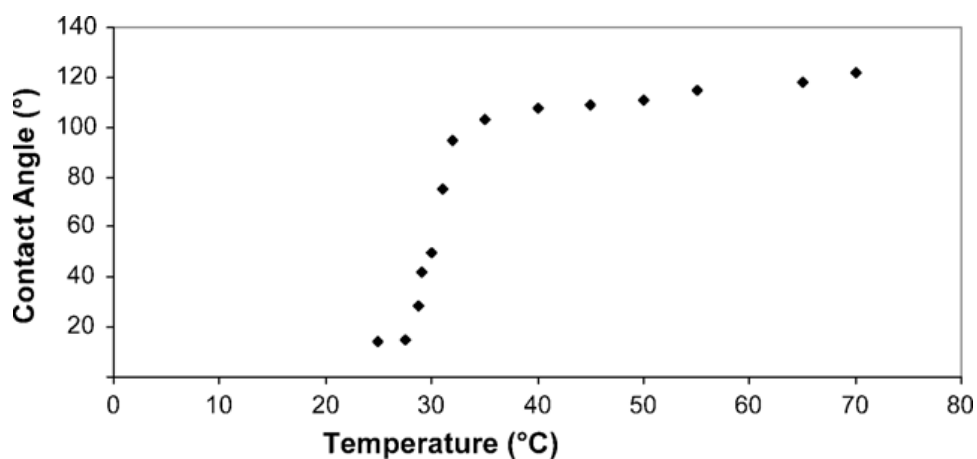


Figure 4.11: Plot of contact angle vs. temperature on the switchable thermosensitive surface.

Figure 4.12 shows the contact angle change of the switchable surface with grafted PNIPAAm. The contact angle decreases as the temperature decreases.

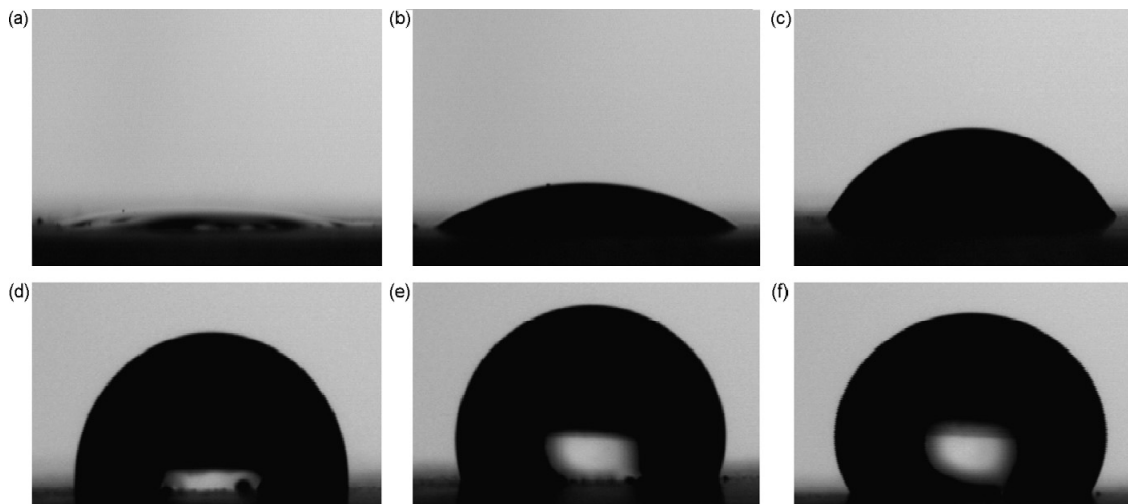


Figure 4.12: Contact angle change with increasing temperature. Temperature increases from (a)-(f): (a) contact angle is 14° at a temperature of 25°C and (f) contact angle is 122° at a temperature of 70°C .

The temperature of a glass substrate with the thermosensitive microfluidic valve is controlled using a hot plate. Dyed water is allowed to flow in the microfluidic channels under capillary action only, to test the capability of the valve to control liquid flow. Figure 4.13 shows the working of the switchable valve at 70°C . At this temperature, the PNIPAAm forms intramolecular hydrogen bonds and becomes hydrophobic. The hydrophobic patch with high contact angle (122°) stops the dyed water at the polymer front. This corresponds to the “closed” status of the valve.

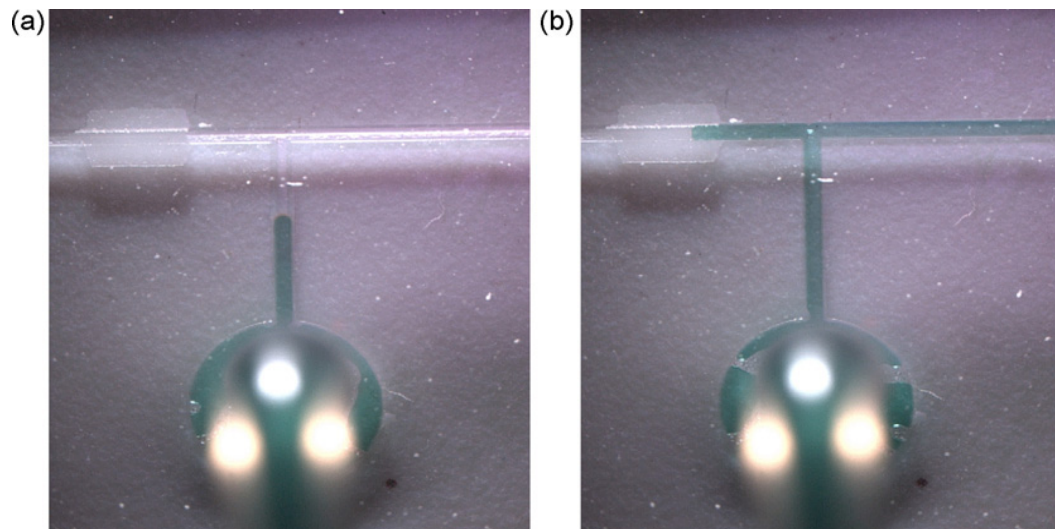


Figure 4.13: "Closed" status of the valve: (a) dyed water approaches junction and (b) water is stopped at hydrophobic polymer surface. The operating temperature is 70 °C.

Figure 4.14 shows the operation of the switchable valve at room temperature where PNIPAAm forms intermolecular hydrogen bonds and becomes hydrophilic. The hydrophilic patch with low contact angle (14°) allows the dyed water to flow through. This corresponds to the "open" status of the valve. These results demonstrate that a switchable thermosensitive valve fabricated from a rough patch functionalized with PNIPAAm is able to manipulate the liquid flow by temperature.

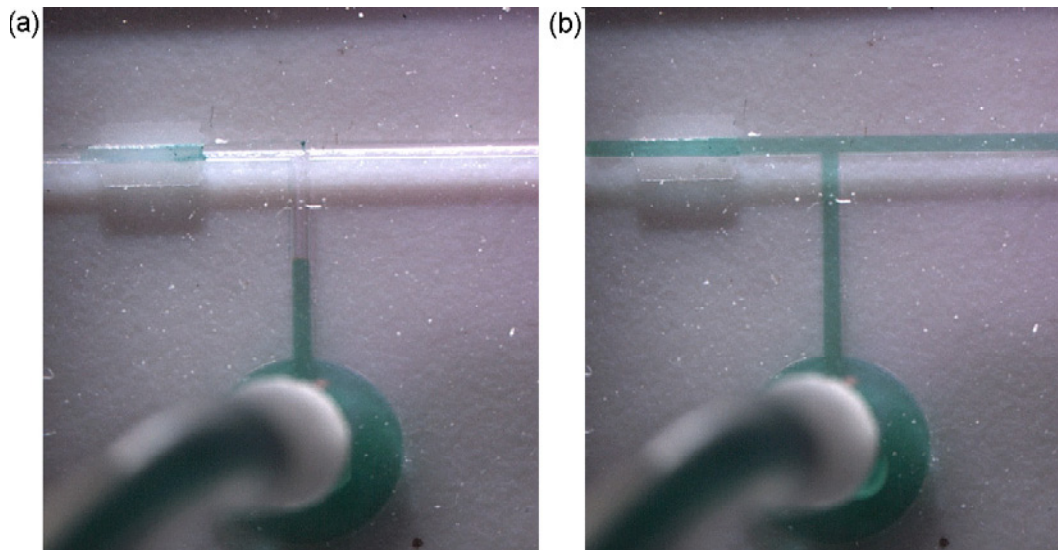


Figure 4.14: "Open" status of the valve: (a) dyed water approaches the junction and (b) water passes over the polymer surface at room temperature as the patch has switched to become hydrophilic.

Sections of multiple microchannels can be selectively deposited with the thermoresponsive polymer patches and integrated with corresponding microheaters. The microheaters can be programmed to turn on or off in a sequential manner which may lead to sophisticated LOC systems and even computational and logical microfluidic circuits [64, 65].

CHAPTER 5: CHARACTERIZATION OF THE SWITCHABLE THERMORESPONSIVE MICROFLUIDIC FLOW REGULATOR

Realizing innovative applications with precision control using the thermoresponsive microfluidic regulator described in CHAPTER 4 requires detailed analysis and characterization studies. Understanding microfluidic behavior which is dominated by viscous and interfacial forces [66, 67] is necessary to develop novel devices. The reported design of hydrophilic-hydrophobic microcanals gives insight for surface energy based liquid flow [68]. Patterning the thermosensitive (PNIPAAm), smart surface in a glass microchannel effectively results in the integration of a switchable hydrophobic patch in the microchannel. This creates a difference in the surface free energy across the advancing meniscus of the liquid front, when it reaches the glass/PNIPAAm contact line, achieving gating of the liquid.

5.1. Device Design

A simple device was fabricated for testing the flow stopping characteristics of the thermoresponsive surface. The device consists of a straight microchannel channel etched in a glass substrate with the switchable thermoresponsive surface selectively deposited in the central portion of the microchannel. The glass patterning and etching process is same as in Chapter 4 (4.2.1). The synthesis of the thermoresponsive surface is described in detail in Chapter 4 (4.3). The microchannel device with the integrated smart surface is

sealed with a flat slab of PDMS by oxygen plasma activation method. The bonded glass PDMS device provides leak proof fluidic flow. PDMS bonding is carried out using a portable held corona treater (Model BD-20AC, Electro-Technic Products Inc.) [69]. The corona treater is used with the disc electrode. The distance between the electrode and the test sample is approximately 0.5 inches. The plasma is adjusted such that it is soft and stable with minimal crackling. Both the glass piece with the microfluidic device and the PDMS piece are treated successively for around 1 minute. Then both the pieces are brought into contact and left overnight on a hotplate at 80 °C [70]. A detailed procedure for the corona treater is described in APPENDIX C.

The fabricated device with the integrated smart surface is shown in Figure 5.1.

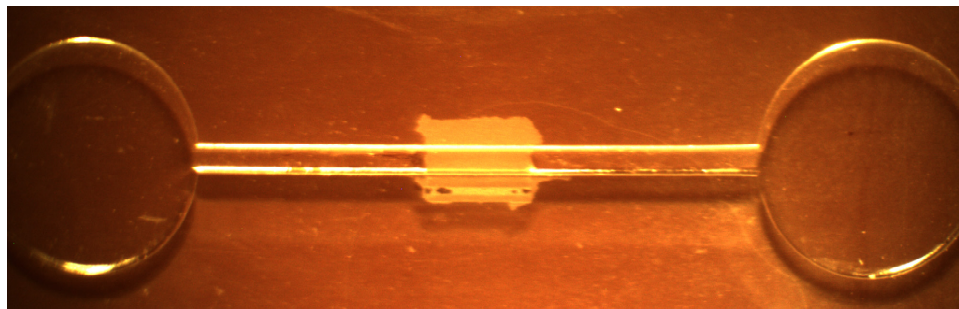


Figure 5.1: The fabricated straight channel microfluidic device in glass substrate with the integrated switchable, nanostructured, thermoresponsive surface (seen as the white patch in the center of the microchannel). Either of the circular reservoirs on each side can be used as the inlet.

SEM micrograph of the cross section of the etched microchannel is shown in Figure 5.2. It was approximated to a trapezium. The width of the microchannel is $b_2 \cong 840 \mu\text{m}$, $b_1 \cong 0.8b_2 = 672 \mu\text{m}$ and the depth is $h \cong 145 \mu\text{m}$. The length of the microchannel is designed in the photolithography mask and is set at $L = 1\text{cm}$.

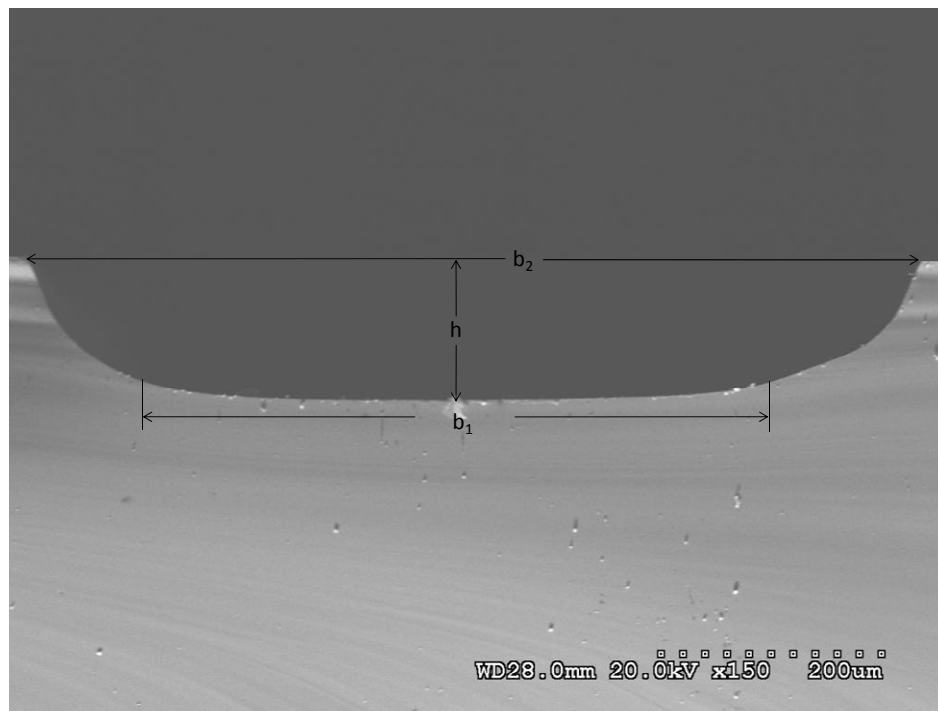


Figure 5.2: SEM micrograph showing the trapezoidal cross section of the microchannel

5.2. Fluid Mechanics in Microdevices

Microfluidic device design must take into consideration the laminar flow regime, very small geometries, the effect of surface energies and complex interplay of pressure gradients and capillarity. A number of interesting fluid-dynamics phenomenon have been reported for microdevices [71].

5.2.1. Dimensionless Numbers to Characterize Microflow

The interfacial force at the solid-liquid-gas contact line and the laminar flow rate has a dominant effect on the fluid flow in a microchannel. The proportion of influence of different forces (i.e., interfacial, viscous, inertial and gravitational) on the fluid guides us in developing efficient design rules for the microdevices. The dimensionless numbers rank the importance of each force and hence classify the multiphase microflows [72].

The capillary number Ca , defined as the ratio of the viscous to the interfacial forces is given by:

$$Ca = \frac{\varepsilon U_d}{\sigma_{LV}} \quad (5.1)$$

where ε is the kinematic viscosity of the fluid and U_d is the linear velocity of the fluid.

The linear fluid velocity is given by:

$$U_d = \frac{R_h^2 \Delta P}{8 \eta L} \quad (5.2)$$

where R_h is the hydraulic radius of the microchannel, ΔP is the pressure difference, η is the dynamic viscosity of the fluid and L is the length of the microchannel. The hydraulic or the wetting radius is defined as:

$$R_h = \frac{A}{P} \quad (5.3)$$

where A and P are the area and perimeter of the microchannel respectively. Since the microchannel used for this study has a trapezoidal cross section as shown in Figure 5.2, the area of the microchannel cross section is:

$$A = \left(\frac{b_1 + b_2}{2} \right) h \quad (5.4)$$

The perimeter of the trapezium is given by:

$$P = b_1 + b_2 + 2 \sqrt{h^2 + \frac{(b_2 - b_1)^2}{4}} \quad (5.5)$$

The dynamic viscosity used in of water used in Equation (5.2) changes with temperature [73] according to the equation:

$$\eta(T) = C_1 10^{\frac{C_2}{(T+273.15)+C_3}} \quad (5.6)$$

where $C_1 = 2.414 \cdot 10^{-5} Pa \cdot s$, $C_2 = 247.8K$ and $C_3 = 140K$ are the constants of the equation and T is the temperature in degree Centigrade (in this case the experiment is carried out at $T = 55$ °C).

The Weber number We , defined as the ratio of the inertial to interfacial forces is given by:

$$We = \frac{\rho U_d^2 L_o}{\sigma_{LV}} \quad (5.7)$$

where ρ is the density of the test liquid and L_o represents the characteristic length of the liquid-gas interface.

Reynolds number, which is perhaps the most frequently used dimensionless number for the characterization of multiphase microflow is given by:

$$Re = \frac{We}{Ca} \quad (5.8)$$

Reynolds number gives the ratio of the inertial to the viscous forces. The laminar flow regime in the microchannels generally falls in the low Reynolds number range indicating that the viscous forces are dominant.

5.2.2. Pressure Differential

Water flows from the inlet to outlet of the fabricated device due to capillary action of the microchannel. When the integrated thermoresponsive surface is heated above its LCST, it becomes hydrophobic and stops the fluid flow along the microchannel. In order for the water to flow over the hydrophobic thermoresponsive patch, pressure is required to drive the laminar flow and to overcome the drop due to surface tension across the advancing meniscus [54]. A schematic of the water meniscus at the glass-PNIPAAm interface is shown in Figure 5.3.

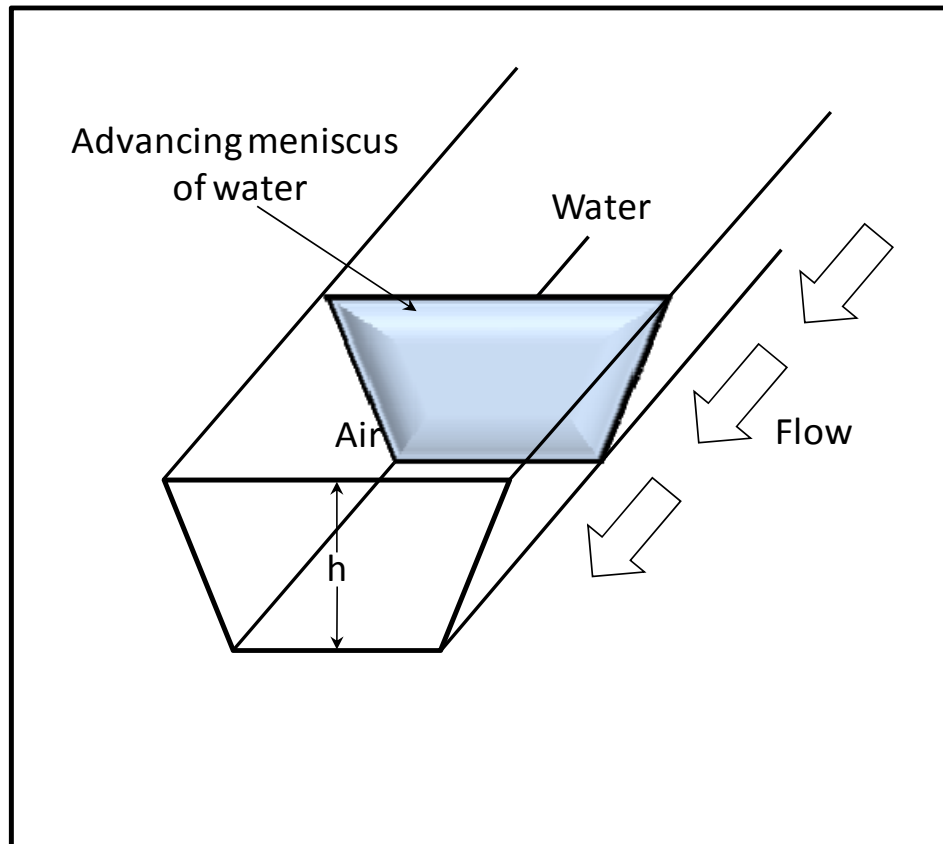


Figure 5.3: Shape of the advancing meniscus of the water at the interface of the glass-PNIPAAm contact line

5.2.2.1. Hagen-Poiseuille Equation

The laminar flow pressure drop is given by the Hagen-Poiseuille equation [37]:

$$\Delta P_L(T) = Q R_f(T) \quad (5.9)$$

We obtain the volumetric flow rate Q from the experimental conditions and the fluidic resistance for a microchannel with trapezoidal circular cross section is given by:

$$R_f(T) = \frac{8 \eta(T) L}{\pi R_h^4} \quad (5.10)$$

The drop due to the laminar flow is negligible as the flow rate is very low due to the fact the water in the microchannel is flowing only due to capillary action.

5.2.2.2. Young-Laplace Equation

The Young-Laplace equation [74, 75] which gives the surface tension pressure drop across the advancing meniscus can be written as:

$$\Delta P_s(T) = \sigma_{LV}(T) \left(\frac{1}{R_1} + \frac{1}{R_2} \right) \quad (5.11)$$

where R_1 and R_2 are the principal radii of curvature of the liquid with respect to the width and height of the microchannel respectively.

Table 5.1 gives the change of the surface tension with temperature [76].

Table 5.1: Variation of the Liquid-Gas Interfacial Energy with Temperature

Temperature (°C)	Liquid-Gas Interfacial Energy (J/m ²)
20	0.07275
30	0.0712
40	0.0696
50	0.06794
60	0.06624
70	0.06447
80	0.06267

The radius of curvature of the liquid with respect to the width in a hydrophobic channel is schematically depicted in Figure 5.4.

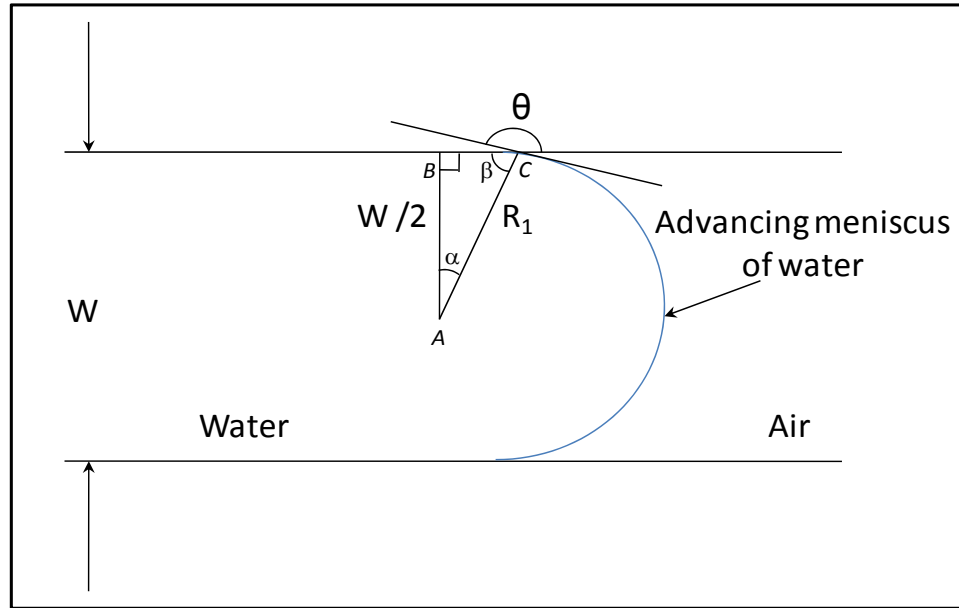


Figure 5.4: Schematic depicting the shape of the principal radius of curvature of the advancing meniscus of water in a hydrophobic channel with respect to the width of the channel.

Since the microchannel has a trapezoidal cross section, the average width of the channel will be $W = \frac{b_1 + b_2}{2}$. The contact angle (θ) of the water with a hydrophobic channel (one could also consider a hydrophilic channel) is defined between the side wall of the channel and a tangent to the advancing meniscus. In triangle ABC , angle $\beta = \theta - 90$ and hence angle $\alpha = (180 - 90) - \beta = 180 - \theta$.

Now, we can write: $\cos(\alpha) = \cos(180 - \theta) = \frac{W}{2R_1}$

Therefore

$$R_1 = -\frac{W}{2 \cos(\theta)} \quad (5.12)$$

Similar argument for the radii of curvature of the liquid of the water with respect to the height of the microchannel leads us to the equation:

$$R_2 = -\frac{h}{2 \cos(\theta)} \quad (5.13)$$

The same geometrical manipulation for a hydrophilic microchannel leads us to radii of curvature similar to Equations (5.12) and (5.13).

Substituting Equations (5.12) and (5.13) in Equation (5.11) we get:

$$\Delta P_s(T) = -2 \sigma_{LV}(T) \cos[\theta(T)] \left(\frac{1}{W} + \frac{1}{h} \right) \quad (5.14)$$

Since the microfluidic channel is a thin capillary [39] and satisfies the condition $W \gg h$, we can approximate the above equation as:

$$\Delta P_s(T) = -2 \sigma_{LV}(T) \cos[\theta(T)] \left(\frac{1}{h} \right) \quad (5.15)$$

Hydrophilic canals patterned on a hydrophobic substrate have been used to establish flow in a streamline. The maximum pressure that the stream of water can withstand without

bursting into the hydrophobic field has been derived using the Young-Laplace equation [77].

Similarly, the maximum pressure P_{max} that the switchable thermoresponsive patch can withstand can be calculated by summation Equations (5.15) and (5.9).

5.3. Measurement Set-up

5.3.1. Calibration of the Pressure Sensor

The pressure in the microfluidic device with the integrated thermoresponsive surface is measured using a two port differential pressure sensor (PX 2300-2DI, Omega Engineering Inc. Stamford, CT). The measured pressure values are logged by a 4 channel voltage recorder (OM-CP-QUADVOLT, Omega Engineering Inc., Stamford, CT) at a fixed frequency. The output voltage is plotted against time on a PC which is interfaced with the voltage recorder. The voltage output of the pressure sensor is calibrated with pressure from a column of water. For this, the high port of the pressure sensor is connected to a burette with centimeter markings. Before measurement, it is ensured that the pressure sensor and the zero value of the water in the burette are at the same level. Water is poured in the burette in increments of 1 cm and the increase in pressure is logged. The calibration curve of the pressure sensor is shown in Figure 5.5.

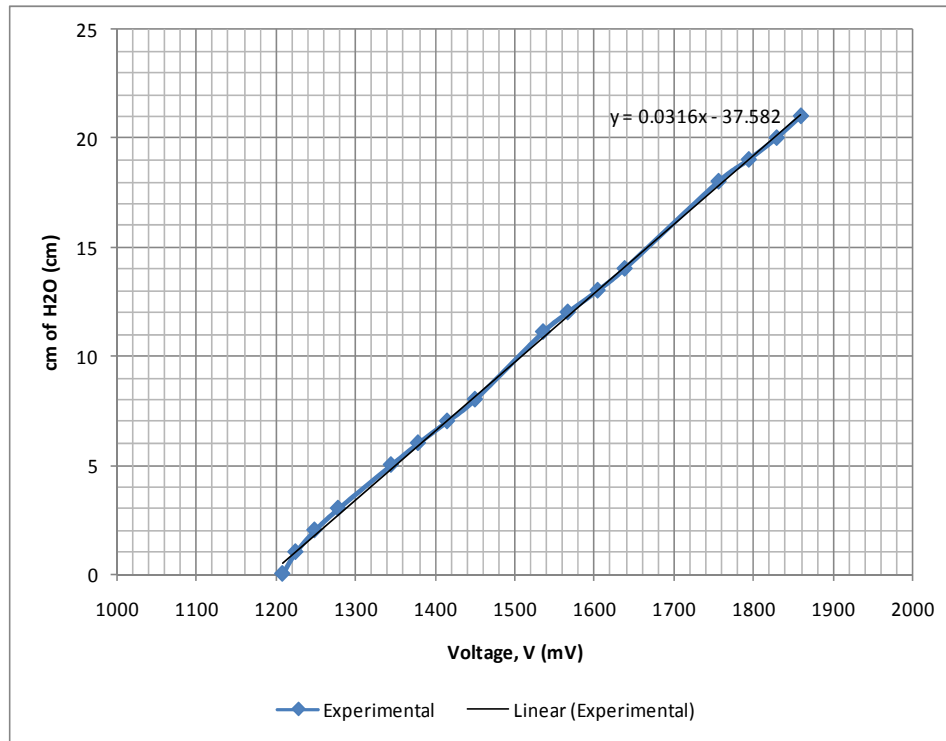


Figure 5.5: Calibration curve for the pressure sensor.

The equation of the linear fit on the curve gives us the slope m_{H_2O} in cm/mV, which will be used in calculating the height (in cm) of the water column as:

$$h_{H_2O} = V m_{H_2O} \tag{5.16}$$

The corresponding differential pressure in pascals is then given by:

$$\Delta P = h_{H_2O} \rho g \quad (5.17)$$

where $g = 9.81m/s^2$ is the acceleration due to gravity.

5.3.2. Differential Pressure Measurement for the Microfluidic Flow Regulator

The schematic of the set up for measuring the differential pressure in the straight microchannel device with the integrated switchable thermoresponsive PNIPAAm coated surface is shown in Figure 5.6. The set up consists of a syringe pump (Harvard PHD 2000) connected through a T junction connector to the microfluidic device inlet and the high port of the differential pressure sensor. The low port of the pressure sensor is left open to the atmospheric pressure corresponding to the pressure at the outlet of the device. The pressure sensor essentially measures the differential pressure of the water flowing in the microchannel.

The picture of the actual set up for measuring the differential pressure in the straight microchannel device with the integrated switchable thermoresponsive PNIPAAm surface is shown in Figure 5.7.

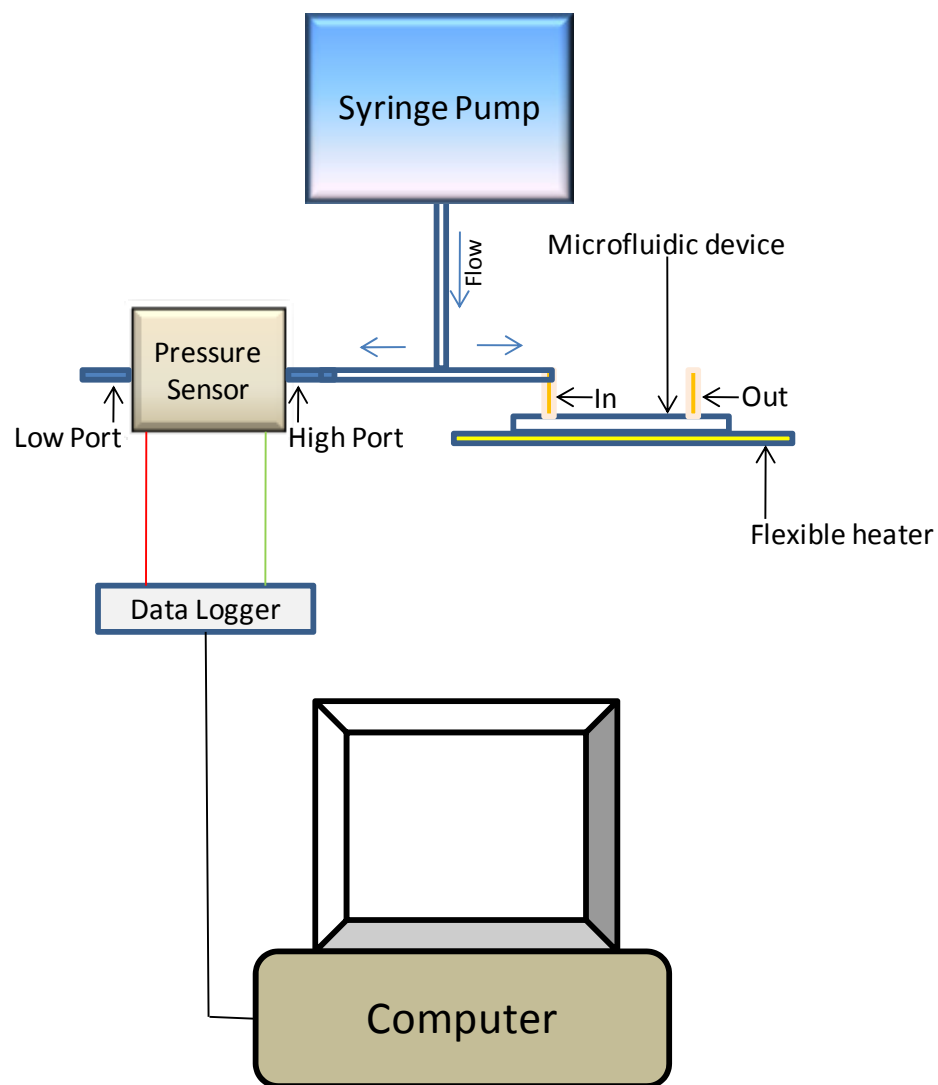


Figure 5.6: Schematic showing the set up for the pressure measurement. In, Out - inlet & outlet respectively of the microfluidic device.

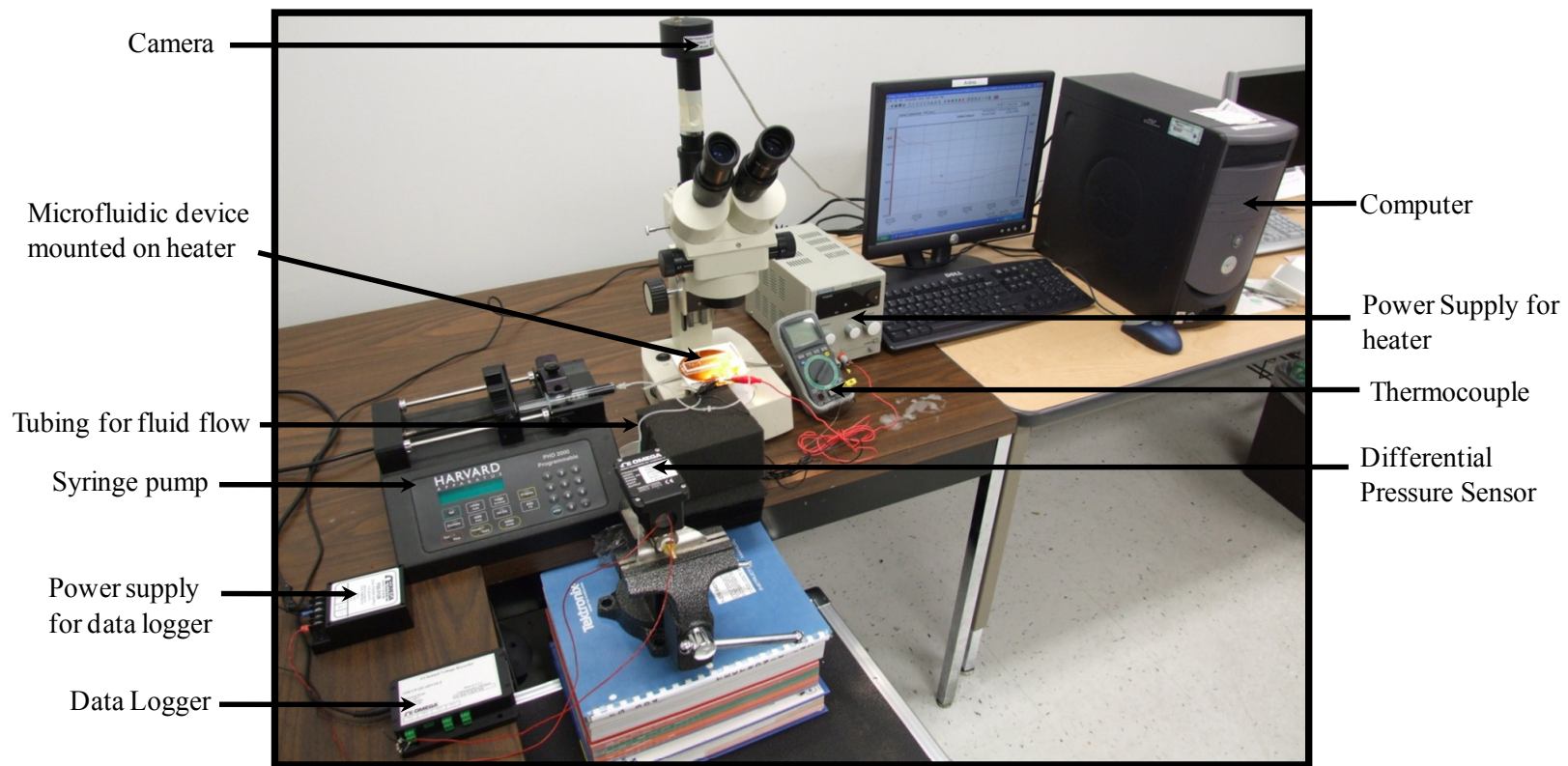


Figure 5.7: Picture of the set for pressure measurement.

The fabricated microfluidic device is attached to a flexible heater which is connected to a DC power supply as shown in Figure 5.8.

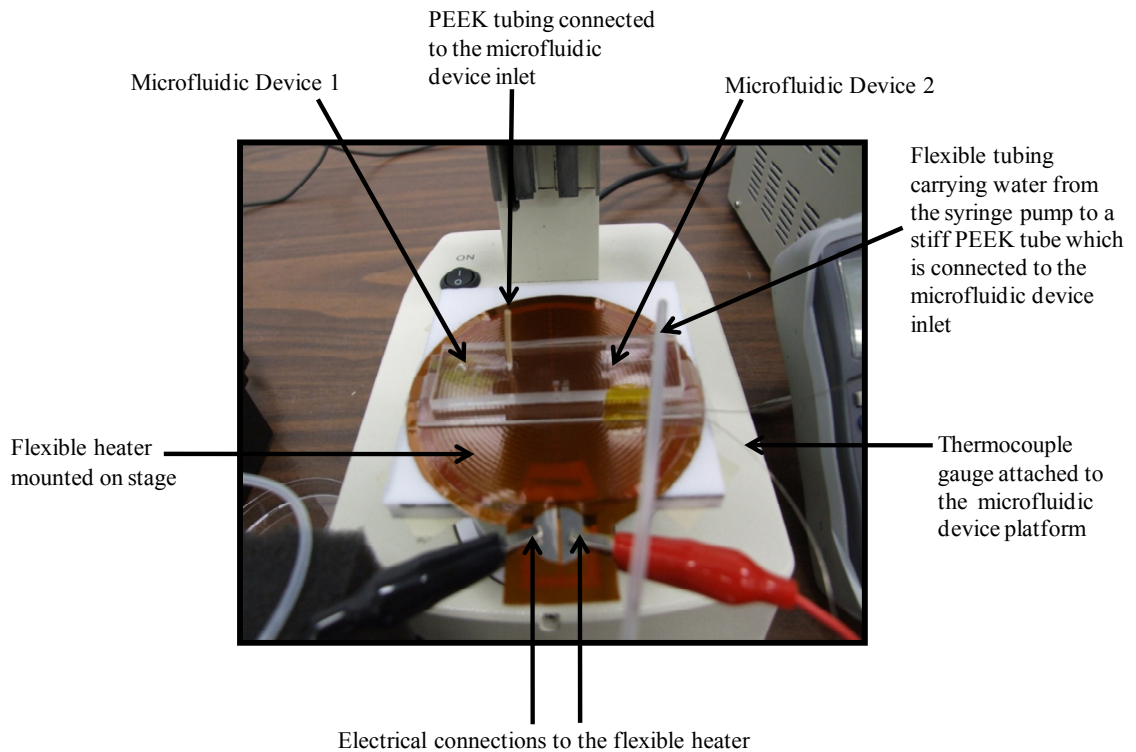


Figure 5.8: Close up view of the microfluidic device mounted on the heater and connected to the pressure sensor for pressure measurement.

A fine gauge thermocouple (Omega Engineering Inc.) is attached to the glass substrate of the microfluidic device and the temperature is constantly monitored throughout the experiment. The microfluidic device, syringe pump and the differential pressure sensor

are arranged at the same height so that the weight of the water column does not create excessive pressure inside the microchannel.

The differential pressure drop that is measured is defined as $\Delta P = P_{in} - P_{out}$, where P_{in} is the pressure at the microfluidic device inlet and P_{out} is the pressure at the device outlet, which in this case is essentially the atmospheric pressure. Water colored with dye is pumped by the syringe pump at a pumping speed of 50 $\mu\text{L/hr}$ till it fills up the inlet reservoir of the microfluidic device. Once the water starts flowing in the microchannel, the external pumping is immediately stopped. Now since the pump and the device are at the same level, the water flows in the microchannel only due to capillary action. The advancing meniscus of the water stops soon after it touches the glass-PNIPAAm contact line. The voltage readings from the pressure sensor converted to pressure differentials and plotted versus time are shown in Figure 5.9. The conversion of voltage output of the sensor to corresponding pressure is described in Section 5.3.1.

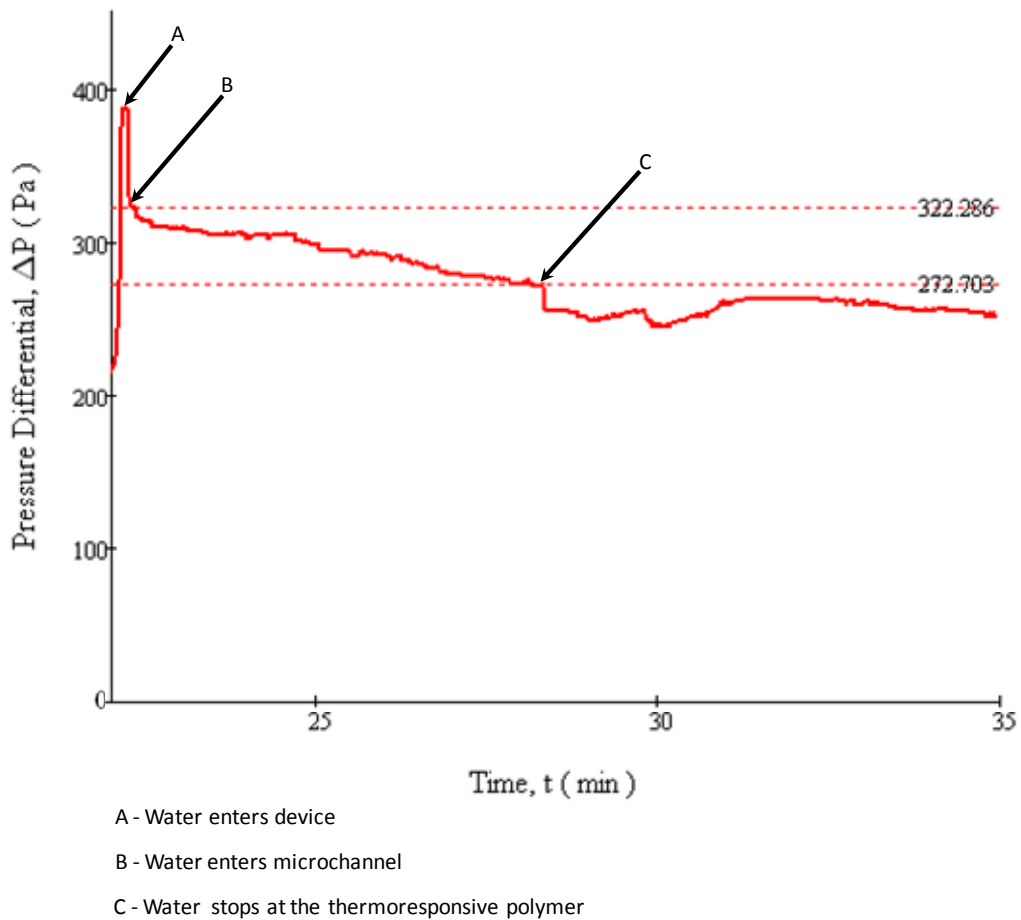


Figure 5.9: Plot of pressure versus time for the straight channel microfluidic device with the integrated thermoresponsive surface. This measurement was carried out at a device temperature of 55 °C when the thermoresponsive surface was hydrophobic.

The water enters the microfluidic device at point (A) in the plot of Figure 5.9. The pressure differential decreases as soon as the water enters the microfluidic device, which is expected, since the water enters the device inlet reservoir which has a larger volume and is made in a hydrophilic glass substrate. As the water starts to flow in the microchannel (point (B) in the plot) under the influence of capillary action, the pressure

steadily decreases till the water front reaches the thermoresponsive polymer surface. The water stops flowing when it comes in contact with the hydrophobic thermoresponsive polymer (point C in the plot).

Two different cases of surface energies arise as the water flows in the microchannel device. The first case is when the water is flowing in the microchannel along glass walls. In this case the two side walls and the lower floor is made of glass while the upper ceiling is made of PDMS. Glass is a hydrophilic material with contact angles (of a water drop) ranging from 10° to 25° and PDMS is a hydrophobic material with a native contact angle of 110° . Since a majority of the walls are hydrophilic, the water experiences overall hydrophilicity and flows in the microchannel inherently under capillary action. This can also be inferred by calculating the capillary number for the microchannel. With the given dimensions, using Equation (5.1), we get $Ca = 0.0007068$. The very low value of the capillary number proves that the interfacial forces dominate and establish a capillary flow.

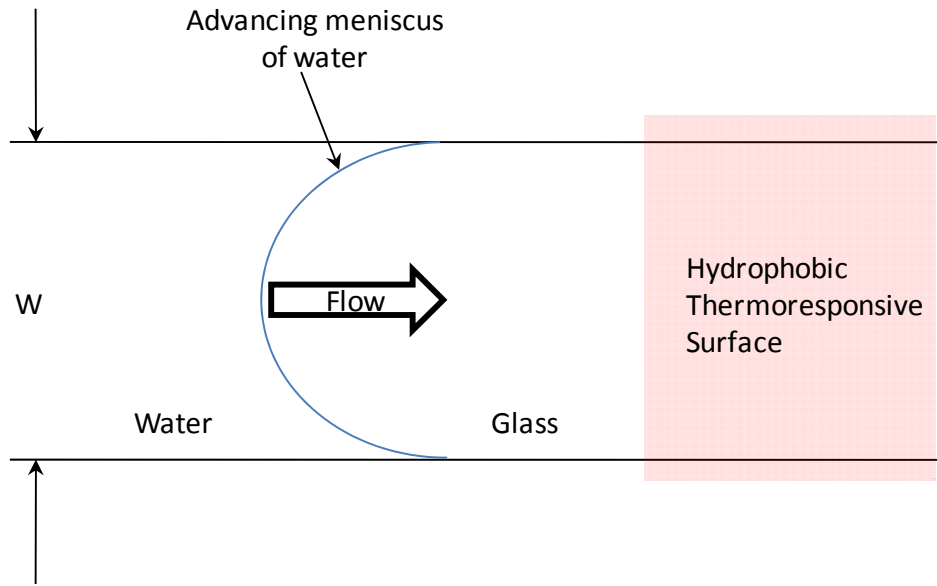
Further, the Weber number for the present device can be calculated from Equation (5.7) as $We = 0.008028$. The characteristic length L_o in Equation (5.7) can be approximated as the hydraulic radius R_h .

As the water flows in the microchannel, it can be seen from Figure 5.9 that the pressure decreases steadily as the flow is in the laminar regime. This is confirmed by calculating the Reynolds number using Equation (5.8). The value of the Reynolds number comes out to be $Re = 11.357$ which proves that the flow in the microchannel is in the laminar regime [78] as expected.

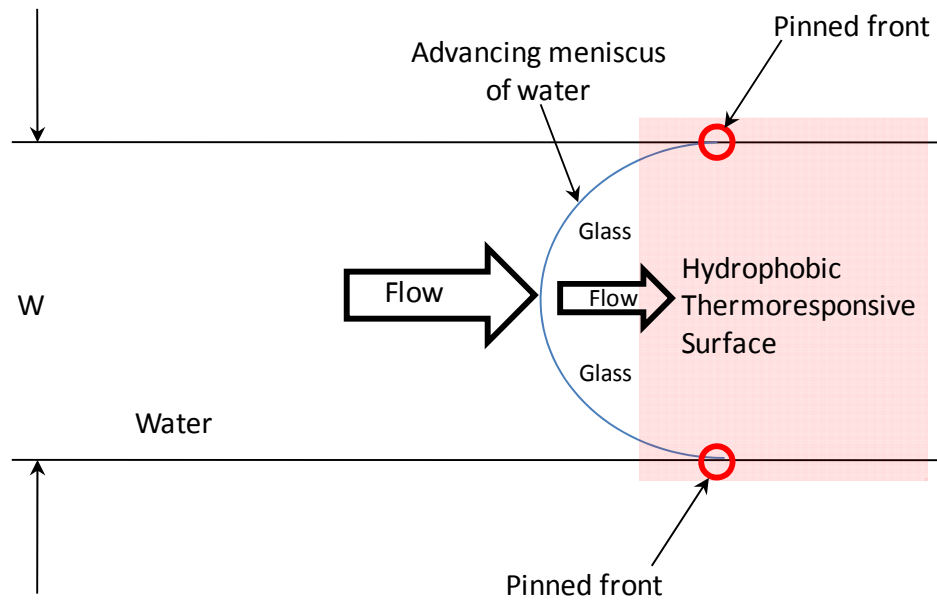
The second case of surface energy consideration occurs when the water front reaches the glass-PNIPAAm contact line. The switchable thermoresponsive PNIPAAm surface is conformally coated on both the side walls and the floor of the glass microchannel. The flow experiment is carried out at a temperature of 55 °C. At this temperature, the contact angle of a water droplet on the switchable thermoresponsive hydrophobic surface is approximately 114°. Now the water encounters three surfaces (two side walls and the floor) which have a contact angle of 114° and the top PDMS ceiling which has a contact angle of 110°. Hence the water front now experiences overall hydrophobicity. This case is shown schematically in Figure 5.3.

It is observed from Figure 5.9 that as soon as the advancing meniscus of the water touches the thermoresponsive surface (point C in the plot) there is a small but abrupt decrease in the pressure differential. This abrupt decrease, though counter intuitive, can be explained by the concept of pseudo-hydrophilicity [79]. As the water is flowing due to

capillarity in the hydrophilic glass channel, the top view of the advancing meniscus profile is concave (when seen from the gas) as shown Figure 5.10 (a). When the advancing meniscus encounters the hydrophobic thermoresponsive polymer, the front ends of the concave radius are pinned to the hydrophobic surface as shown in Figure 5.10 (b). Due to the pinning, the body of water mass which is still on the hydrophilic glass surface is suddenly forced forward till it encounters the hydrophobic thermoresponsive surface. This sudden forward flow is manifested as a decrease in the pressure differential. The advancing meniscus of the water after it has been stopped by the hydrophobic thermoresponsive surface is shown in Figure 5.10 (c). The meniscus has to maintain contact with the walls of the microchannel but cannot move forward over the hydrophobic surface and attain a hydrophobic convex shape. It can still be viewed as a static hydrophilic front and hence the name pseudo-hydrophilicity.



(a)



(b)

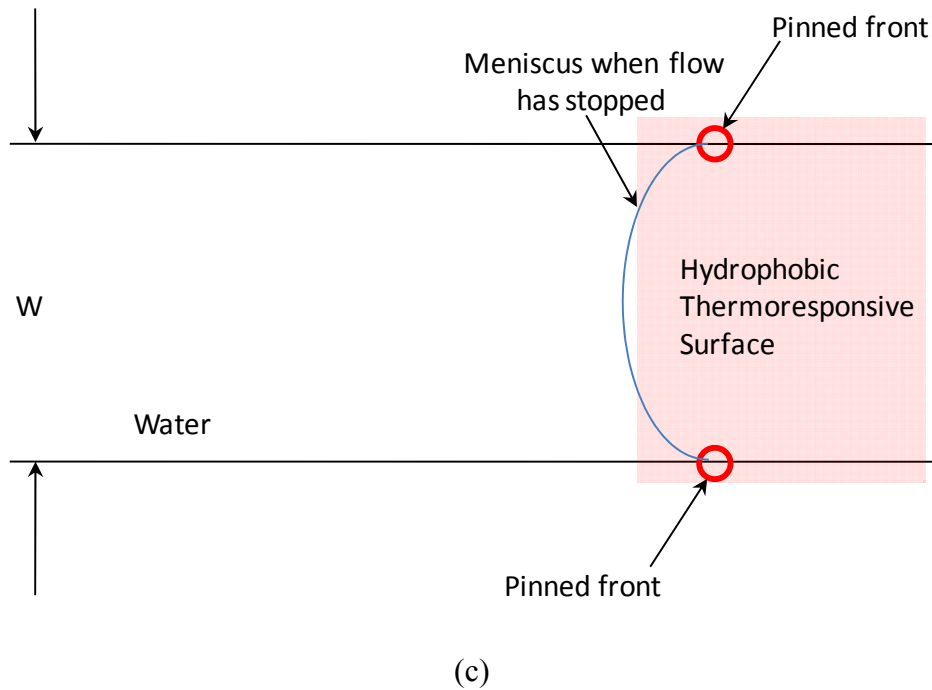


Figure 5.10: Schematic of the changing radius of curvature of the advancing meniscus of water flowing under capillary action in the microchannel. (a) Concave principal radii of curvature of water when it is flowing in the glass channel indicating that the water front experiences overall hydrophilicity. (b) Radius of curvature when the advancing meniscus of water reaches the glass-hydrophobic thermoresponsive surface interface. The front ends of the water meniscus are pinned to the hydrophobic surface. Due to this pinning action, the body of water is suddenly pushed toward the hydrophobic surface giving rise to an abrupt drop in the pressure differential. (c) The advancing meniscus of water after it has been stopped by the thermoresponsive hydrophobic surface. The shape of the meniscus is still slightly concave (or may be flat at the most), as the water cannot pass over the hydrophobic surface ahead.

According to the mathematical analysis of the maximum pressure that the hydrophobic thermoresponsive valve can withstand is presented in Section 5.2.2, the maximum pressure is given by:

$$P_{max}(T) = -2 \sigma_{LV}(T) \cos[\theta(T)] \left(\frac{1}{h}\right) + Q \frac{8 \eta(T) L}{\pi R_h^4} \quad (5.18)$$

Since the fluid is flowing in the microchannel only under capillary action, we can assume a very low flow rate like $Q = 10 \mu L/hr$. The dimensions of the channel are known from Section 5.1 as $L = 1 cm$, $b_2 \cong 840 \mu m$, $b_1 \cong 0.8 b_2 = 672 \mu m$ and $h \cong 145 \mu m$. The hydraulic radius is found from Equation (5.3) as $R_h = 59.346 \mu m$. The experiment is carried out at a temperature of $T = 55 \text{ }^\circ C$. The value of the dynamic viscosity at this temperature can be obtained from Equation (5.6) as $\eta = 5.009 \cdot 10^{-4} kg/m s$.

The liquid-vapor interfacial energy at the operating temperature can be obtained from Table 5.1 as $\sigma_{LV} \cong 0.068 J/m^2$. The value of the contact angle of a water droplet on the thermoresponsive surface at $T = 55 \text{ }^\circ C$ can be obtained from Equation (2.5) (CHAPTER 2) as $\theta(55 \text{ }^\circ C) = 114.2^\circ$. At the point when the flow is stopped, the front meniscus of water is in between the thermoresponsive surface and a PDMS ceiling. Since PDMS has a native contact angle of 110° , we can take the average contact angle as $\theta = \frac{114.4^\circ + 110^\circ}{2} = 112.2^\circ$. Using all the above parameters in Equation (5.18), we obtain the maximum pressure that the hydrophobic thermoresponsive surface can withstand as $P_{max} = 356.933 Pa$. Several attempts have been reported to combine micro and nano fluidic components to achieve adequate pressure and flow rates. The low value of P_{max} implies that the thermoresponsive material alone cannot provide adequate pressure

withstanding capability when used in a microfluidic valve. The thermoresponsive material has to be used with other valving concepts to achieve adequate pressure and flow rates [80].

The contact angle of a water droplet on the thermoresponsive surface, at a range of temperatures from 25 °C to 70 °C can be measured by using a standard goniometer. Equation (5.15) can then be used to calculate the Young-Laplace pressure differential corresponding to the changing contact angles at every incremental temperature rise.

The values of the calculated surface tension pressure differentials and the measured contact angles at various temperatures are shown Figure 5.11.

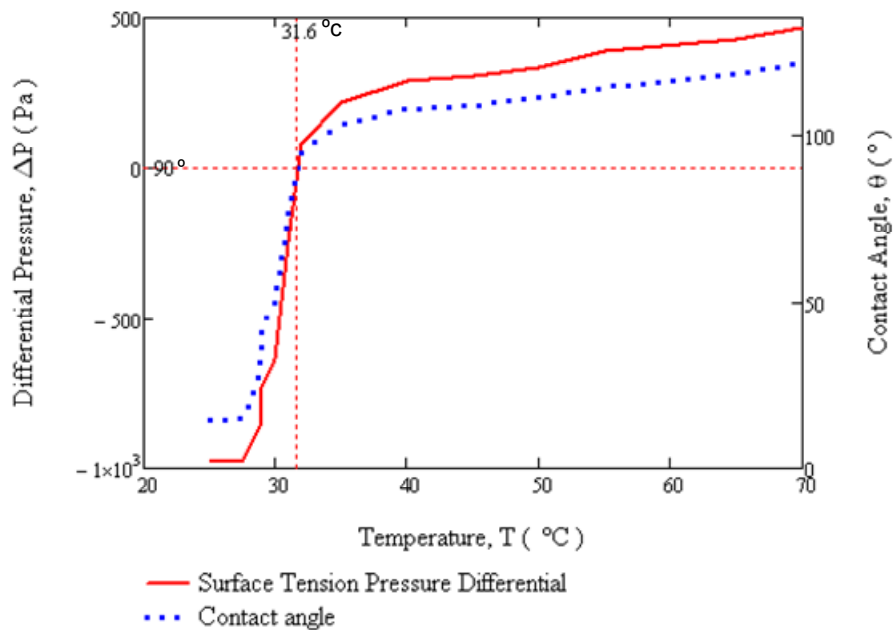


Figure 5.11: Variation of surface tension pressure differential and contact angle with change in temperature of the integrated thermoresponsive surface in the microfluidic flow regulator

It can be seen from Figure 5.11 that the pressure differential becomes positive when the contact angle $\theta \geq 90^\circ$. Positive pressure differential implies hydrophobic surface which is capable of fluid flow regulation.

The value of the pressure differential which is negative at 25 °C reflects the fact that the integrated thermoresponsive polymer surface is hydrophilic at room temperature. This

was experimentally verified where a capillary flow is established in the microfluidic device at room temperature and it was observed that the thermoresponsive surface allowed the water to flow over it. The pressure differential readings are plotted versus time in Figure 5.12. We can note that there is no abrupt drop in pressure due to flow stoppage. The pressure steadily decreases due to laminar flow once it enters the microchannel (point B in the plot) till it reaches the outlet reservoir.

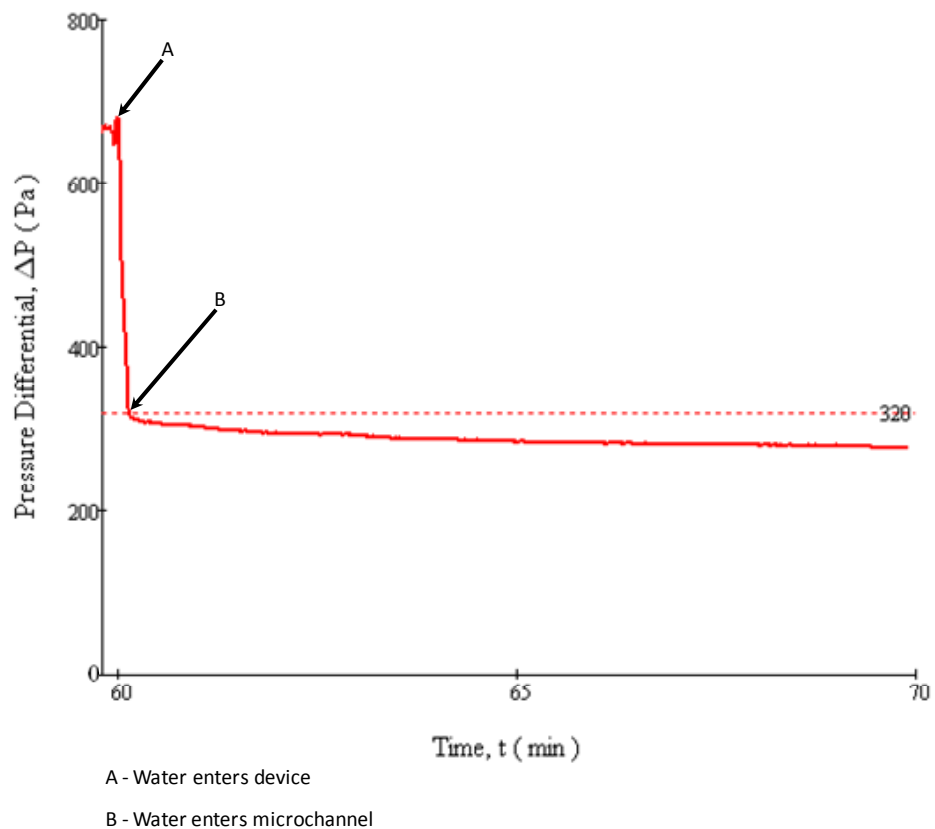


Figure 5.12: Plot of pressure versus time for the straight channel microfluidic device with the integrated thermoresponsive surface. This measurement was carried out at room temperature when the thermoresponsive surface was hydrophilic.

Hence a gating action is achieved in a microfluidic channel by integrating a temperature responsive polymer which is hydrophobic at elevated temperatures (above 33 °C) and hydrophilic at room temperatures.

Using the preceding analysis, we can deduce specifications (as shown in Table 5.2) for the switchable thermoresponsive flow regulator -

(a) Having dimensions of $L = 1\text{cm}$, $b_2 \cong 840\ \mu\text{m}$, $b_1 \cong 0.8b_2 = 672\ \mu\text{m}$ and $h \cong 145\ \mu\text{m}$;

(b) Having a trapezoidal cross section and

(c) Operating at a temperature of 55 °C

Table 5.2: Specifications of the switchable thermoresponsive valve

<i>Parameter</i>	<i>Value</i>
Flow	Capillary flow
Hydraulic Radius	59.346 μm
Capillary number	0.0007068
Weber number	0.008028
Reynolds number	11.357
Maximum pressure that can be stopped at a temperature of 55 °C	356.933Pa
Minimum Operating Temperature	$\approx 33\text{ }^\circ\text{C}$
Minimum required contact angle of the thermoresponsive surface for flow regulation	100°

CHAPTER 6: CONCLUSION AND FUTURE WORK

This work explored the modeling of a thermoresponsive material for the applications in microfluidic devices and exploited the defined characteristics for a flow regulating function in the fabricated devices. Different types of devices were realized and tested to provide comprehensive solutions for the integration of nanostructured thermoresponsive polymers into microchannels.

A detailed theory of the switchable, nanostructured, thermoresponsive PNIPAAm surface was developed and mathematical equations were derived for calculating - the contact angle of a water droplet at any given temperature, the gain of the thermoresponsive surface, the exact value of the LCST and the beginning and end of the LCST range. The proposed mathematical model, analysis and expressions can be generalized for any kind of thermoresponsive surface which exhibits a transfer characteristic that can be fitted to a sigmoidal logistic function. This work will potentially lay the basis for identifying and understanding the wettability switching characteristics of thermosensitive polymers.

By incorporating the appropriate roughness, introducing low surface energy material and grafting the thermosensitive polymer PNIPAAm, a tunable surface for wettability control was created. Thin film microheaters have been integrated into the smart platform for

controlling the surface temperature of the PNIPAAm. The contact angle of a water droplet can be tuned from the hydrophilic to the hydrophobic domain via the temperature rise provided by the integrated microheater. A platform with a thermosensitive polymer for surface energy manipulation and contact angle tuning integrated with a microheater has been presented. Functional characteristics such as time response, contact angle gain and normalized gain have been studied as groundwork for the further development of thermosensitive polymer based devices and systems.

As a proof of concept devices, microfluidic flow regulators based on superhydrophobic nanostructures and switchable thermosensitive polymer were fabricated and tested, in which multiple bilayers of PAH/PAA and silica nanoparticles were conformally and selectively coated by the LBL deposition technique on a channel wall and used as an integrated gating component. The deposition process was optimized in order that the polyelectrolyte films may be integrated and used as a functional component for microfluidic devices and systems.

The pressure differential measurements carried out on the straight channel microfluidic device with the integrated thermoresponsive polymer gives much needed insight into the potential applications of thermoresponsive materials. The maximum pressure differential that the thermoresponsive flow regulator could withstand was calculated. The

characterization of the flow by the dimensionless numbers (namely the capillary, Weber and Reynolds number) indicates that this kind of flow regulator can be further optimized.

This work as a whole promises the integration of various regulatory functions into lab-on-a-chip devices using a wide range of available polyelectrolyte combinations.

Based on this work, the future efforts can be directed to create an array of microheaters integrated with the thermoresponsive surface for parallel/serial programmable flow regulators on a chip.

The LBL deposition technique discussed in this work can be extended and adapted to coat polyelectrolytes or charged species on the inner walls of hollow capillaries. This FLBL (Flow through layer by layer) deposition technique is currently being designed, assembled and tested using a novel micropumping system. Inner walls of glass capillaries were coated with polyelectrolytes and then chemically treated to create a surface for chemical or biological experiments.

APPENDIX A: RCA CLEANING

This appendix describes the RCA cleaning method that can be used to effectively clean silicon and glass.

Equipment:

- 1) 2 Glass beakers, one each for the SC-1 and SC-2 cleaning.
- 2) Hotplate
- 3) Teflon wafer/sample holder

Chemicals:

- 1) Ammonium Hydroxide
- 2) Hydrochloric acid
- 3) Hydrogen Peroxide

It cleaning process has two steps:

1) Standard cleaning 1 (SC-1):

This cleans all organic contaminants.

The solution consists of the following:

6:1:1 – DI Water: Ammonium Hydroxide (NH₄OH): Hydrogen Peroxide(H₂O₂).

Cleaning Procedure:

- 1) Heat DI water and ammonium hydroxide to about 80⁰C.
- 2) Then add hydrogen peroxide. Now the solution will start bubbling.
- 3) Immerse your samples in the SC-1 solution. Keep the sample immersed in the solution for about 10/15 mins (until the solution stops bubbling).
- 4) Take the samples out of the SC-1 solution; rinse with DI water for 5 minutes and blow dry with Ni gun.

2) Standard cleaning 2 (SC-2):

This cleans all metallic contaminants.

The solution consists of the following:

6:1:1 – DI Water: Hydrochloric Acid (HCl): Hydrogen Peroxide (H₂O₂).

Cleaning Procedure:

- 1) Heat DI water and hydrochloric acid to about 80⁰C.
- 2) Then add hydrogen peroxide. Now the solution will start bubbling.
- 3) Immerse your samples in the SC-2 solution. Keep the samples immersed in the solution for about 10mins/15mins (until the solution stops bubbling).
- 4) Take the samples out of the SC-1 solution; rinse with DI water for 5 minutes and blow dry with Ni gun.

If we are cleaning ceramic samples then we have to use only SC-1 cleaning process as the HCl in SC-2 attacks the ceramic.

APPENDIX B: GLASS ETCHING FOR MICROCHANNEL FABRICATION

This appendix describes the recipe for etching glass to create a very smooth profile suitable for microfluidic devices.

Equipment:

- 1) Teflon Beaker
- 2) Stirring hot plate
- 3) Magnetic stirrer
- 4) Wafer holder
- 5) Stand and clamp for the wafer holder

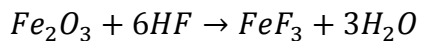
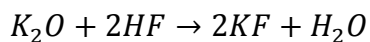
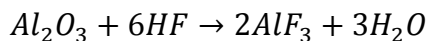
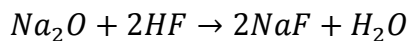
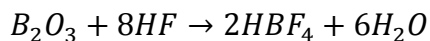
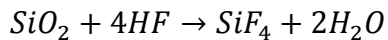
Chemicals:

- 1) Sulfuric acid (H_2SO_4)
- 2) Hydrofluoric acid (HF)
- 3) DI water

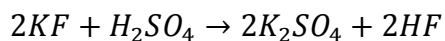
Procedure:

- 1) Use a paint brush to paint the photoresist (PR), Shipley 1813, on the substrate (e.g. silicon wafer).
 - 2) Stick glass slide to Si wafer. Paint Shipley 1813 on the sides of the glass slide to ensure that the sides are totally sealed.
 - 3) Leave for at least 12 hours.
 - 4) Hard bake the Si wafer (with glass sample/s stuck to it) for 10 minutes at 100⁰C.
 - 5) Prepare the glass etching solution as follows:
Mix HF : H₂SO₄ : DI H₂O in the ratio 0.8%(vol) : 32%(vol) : 67.2%(vol) respectively. Following the above ratios, typically we would mix 6.4ml of HF, 256ml of H₂SO₄ and 537.6ml of DI H₂O.
- Note: Always add acid to water. This is an exothermic reaction. Leave the solution at RT for at least 1 hour for cooling.**
- 7) The Etch rate of this solution for Pyrex (Borofloat) glass is around 0.08 to 0.1µm/min.
 - 8) The etching is carried out at a stir speed of 600rpm and temperature of around 25 °C.

The following chemical reactions take place in the glass etch:



All the metal fluorides are soluble in water except the fluorides of aluminum and potassium. The purpose of the sulfuric acid is to convert the fluorides of aluminum and potassium into the respective sulfates. The sulfates of these metals are soluble in water.



APPENDIX C: GLASS-PDMS BONDING USING CORONA TREATER

Equipment:

- 1) Corona treater (Model BD-20AC, Electro-Technic Products Inc.)
- 2) Stand with clamp for the corona treater
- 3) Disc electrode of the corona treater
- 4) Flat circular conducting metal plate (Diameter ≈ 5 ")
- 5) Non-conducting Styrofoam block (Dimensions ≈ 12 " x 6 " x 2 ")
- 6) Measuring tape

Procedure:

Note:

This is a high voltage RF equipment. It should not be operated in the vicinity of electronic circuits. It can reset or permanently damage sensitive electronic components.

Do not wear any metallic rings, bracelets, pendants/necklaces or any other ornaments while using this equipment. The high voltage plasma should be operated very carefully.

- 1) Fix the disc electrode to the bottom of the corona treater.
- 2) Fix the corona treater (with the disc electrode affixed) in an upright vertical position using the clamp and stand.
- 3) The metal plate should be placed on a non-conducting platform like a Styrofoam block. The entire block (with the metal plate on top) is now positioned such that the flat circular metal plate is directly beneath the disc electrode.
- 4) Adjust the height of the clamp (on the stand) holding the corona treater, such that the bottom of the disc electrode is approximately 0.5" above the metal plate. Use the measuring tape to measure the distance between the electrode and the metal plate.
- 5) Turn on the high power RF supply and set up the plasma between the disc electrode and the metal plate underneath it. The air-plasma appears like a blue flame and can be adjusted by using the knob on top of the corona treater.

Note: The disc electrode is subjected to very high voltage (in the range of 10kV) to ionize the surrounding air. Do not touch the electrode or the metal plate when the plasma is struck.

- 6) Adjust the top knob to increase or decrease the plasma. The plasma increases when the knob is turned in the anticlockwise direction and the plasma decreases

when the knob is turned in the clockwise direction. Ensure that the plasma is soft and stable. The plasma should produce minimum crackling.

- 7) Now turn off the RF power supply.
- 8) Place the glass substrate to be bonded on the metallic plate not directly underneath the plasma electrode.
- 9) Turn on the RF supply and strike a soft stable plasma between the electrode and the metal plate by readjusting the top knob.
- 10) Once a typical plasma is formed, move the Styrofoam block such that glass sample (on the metal plate) is directly underneath the electrode in the plasma field.
- 11) Move the Styrofoam block back and forth such that the plasma irradiates all parts of the glass sample. This process needs to be carried out for at least 1 minute for a 3" x 1" sample.
- 12) At the end of 1 minute turn off the RF power supply and remove the glass sample from the metal plate.
- 13) Now repeat the same process (steps 8 to 12) for the flat piece of fresh clean PDMS.

14) Once the plasma activation for both the glass sample and the flat PDMS slab is done, bring both the pieces in conformal contact. Do not press the PDMS too hard on the glass sample. Press gently to make sure that there are no air pockets between the glass and the PDMS.

15) Place the Glass-PDMS pieces (which are in intimate contact with each other) on a hotplate at 80 °C and leave overnight.

16) Complete bonding will occur after about 8 hours.

REFERENCES

- [1] A. McWilliams, "Nanotechnology: A Realistic Market Assessment," July 2006.
- [2] W. F. Brinkman, D. E. Haggan, and W. W. Troutman, "A History of the Invention of the Transistor and Where It Will Lead Us," *IEEE J. Solid-State Circuits*, vol. 32, pp. 1858-1865, 1997.
- [3] M. Madou, *Fundamentals of Microfabrication*: CRC Press, 1997.
- [4] O. K. Varghese, D. Gong, M. Paulose, K. G. Ong, E. C. Dickey, and C. A. Grimes, "Extreme Changes in Electrical Resistance of Titania Nanotubes with Hydrogen Exposure," *Advanced Materials*, vol. 15, pp. 624-627, April 17 2003.
- [5] Z. Gu, Y. Chen, and D. H. Gracias, "Surface Tension Driven Self-Assembly of Bundles and Networks of 200 nm Diameter Rods Using a Polymerizable Adhesive," *Langmuir*, vol. 20, pp. 11308-11311, 2004.
- [6] S. Shingubara, "Fabrication of Nanomaterials Using Porous Alumina Templates," *Journal of Nanoparticle Research*, vol. 5, pp. 17-30, 2003.
- [7] B. Michel, A. Bernard, A. Bietsch, E. Delamarche, M. Geissler, D. Juncker, H. Kind, J.-P. Renault, H. Rothuizen, H. Schmid, P. Schmidt-Winkel, R. Stutz, and H. Wolf, "Printing meets lithography: Soft approaches to high-resolution," *IBM J. Res. Develop.*, vol. 45, pp. 697-719, 2001.
- [8] Y. Xia and G. M. Whitesides, "Soft Lithography," *Annu. Rev. Mater. Sci.*, vol. 28, pp. 153-184, 1998.
- [9] J. A. Liddle, L. R. Harriott, A. E. Novembre, and W. K. Waskiewicz, "SCALPEL: A Projection Electron-Beam Approach to Sub-Optical Lithography".

- [10] H. C. Pfeiffer and W. Stickel, "PREVAIL—An E-Beam Stepper with Variable Axis Immersion Lenses," *Microelectronic Engineering*, vol. 27, pp. 143-146, 1995.
- [11] R. D. Piner, J. Zhu, F. Xu, S. Hong, and C. A. Mirkin, "Dip-Pen Nanolithography," *SCIENCE*, vol. 283, pp. 661-663, 1999.
- [12] G. M. Londe, A. Han, and H. J. Cho, "MEMS for Nanotechnology - Top-Down Perspective," in *Functional Nanostructures: Processing, Characterization and Applications*, S. Seal, Ed.: Springer 2007.
- [13] D. A. LaVan, T. McGuire, and R. Langer, "Small-scale Systems for In Vivo Drug Delivery," *Nature Biotechnology*, vol. 21, pp. 1184-1191, 30September 2003 2003.
- [14] A. C. N. Nath, "Creating "Smart" Surfaces Using Stimuli Responsive Polymers," *Advanced Materials*, vol. 14, pp. 1243-1247, 2002.
- [15] Y. Liu, L. Mu, L. B., S. Zhang, P. Yang, and J. Kong, "Controlled Protein Assembly on a Switchable Surface.," *Chem Communications*, vol. 10, pp. 1195-1195, 2004 May 21 2004.
- [16] N. Malmstadt, A. S. Hoffman, and P. S. Stayton, ""Smart" mobile affinity matrix for microfluidic immunoassays," *Lab on a Chip*, vol. 4, pp. 412-415, 2004.
- [17] G. Londe, A. Chunder, A. Wesser, L. Zhai, and H. J. Cho, "Microfluidic valves based on superhydrophobic nanostructures and switchable thermosensitive surface for lab-on-a-chip (LOC) systems," *Sensors and Actuators B: Chemical*, vol. 132, pp. 431-438, 2008.
- [18] J. Xi, J. J. Schmidt, and C. D. Montemagno, "Self-assembled microdevices driven by muscle," *Nat Mater*, vol. 4, pp. 180-184, 2005.
- [19] D. Kuckling, C. D. Vo, and S. E. Wohlrab, "Preparation of Nanogels with Temperature-Responsive Core and pH-Responsive Arms by Photo-Cross-Linking," *Langmuir*, vol. 18, pp. 4263-4269, 2002.

- [20] G. V. Rama Rao, M. E. Krug, S. Balamurugan, H. Xu, Q. Xu, and G. P. Lopez, "Synthesis and Characterization of Silica-Poly(N-isopropylacrylamide) Hybrid Membranes: Switchable Molecular Filters," *Chem. Mater.*, vol. 14, pp. 5075-5080, 2002.
- [21] J. Lahann, S. Mitragotri, T.-N. Tran, H. Kaido, J. Sundaram, I. S. Choi, S. Hoffer, G. A. Somorjai, and R. Langer, "A Reversibly Switching Surface," *Science*, vol. 299, pp. 371-374, 17 January 2003 2003.
- [22] T. Sun, G. Wang, L. Feng, B. Liu, Y. Ma, L. Jiang, and D. Zhu, "Reversible Switching between Superhydrophilicity and Superhydrophobicity," *Angewandte Chemie International Edition*, vol. 43, pp. 357-360, 2004.
- [23] L. M. McDowall and R. A. L. Dampney, "Calculation of threshold and saturation points of sigmoidal baroreflex function curves," *Am J Physiol Heart Circ Physiol*, vol. 291, pp. H2003-2007, October 1, 2006 2006.
- [24] D. Wlodzislaw and J. Norbert, "Survey of Neural Transfer Functions," *Neural Computing Surveys* vol. 2, pp. 163-212, 1999.
- [25] H. Chun-Wei and L. Gwo-Bin, "A microfluidic system for automatic cell culture," *Journal of Micromechanics and Microengineering*, p. 1266, 2007.
- [26] A. Ichikawa, F. Arai, and T. Fukuda, "Optical Temperature Control of Multiple Microheaters Using Digital Micromirror Device," in *Micro Electro Mechanical Systems, 2006. MEMS 2006 Istanbul. 19th IEEE International Conference on*, 2006, pp. 390-393.
- [27] T. Okano, N. Yamada, M. Okuhara, H. Sakai, Y. Sakurai, and D. F. Williams, "Mechanism of cell detachment from temperature-modulated, hydrophilic-hydrophobic polymer surfaces," in *The Biomaterials: Silver Jubilee Compendium* Oxford: Elsevier Science, 2006, p. 109.
- [28] C. H. Ahn, C. Jin-Woo, G. Beaucage, J. H. Nevin, L. Jeong-Bong, A. Puntambekar, and J. Y. Lee, "Disposable smart lab on a chip for point-of-care clinical diagnostics," *Proceedings of the IEEE*, vol. 92, pp. 154-173, 2004.

- [29] S. H. Lee, C. S. Lee, B. G. Kim, and Y. K. Kim, "Quantitatively controlled nanoliter liquid manipulation using hydrophobic valving and control of surface wettability," *Journal of Micromechanics and Microengineering*, p. 89, 2003.
- [30] C. G. J. Schabmueller, M. Koch, M. E. Mokhtari, A. G. R. Evans, A. Brunnschweiler, and H. Sehr, "Self-aligning gas/liquid micropump," *Journal of Micromechanics and Microengineering*, p. 420, 2002.
- [31] W. I. Jang, C. A. Choi, C. H. Jun, Y. T. Kim, and M. Esashi, "Surface micromachined thermally driven micropump," *Sensors and Actuators A: Physical*, vol. 115, pp. 151-158, 2004.
- [32] C. J. Morris and F. K. Forster, "Low-order modeling of resonance for fixed-valve micropumps based on first principles," *Microelectromechanical Systems, Journal of*, vol. 12, pp. 325-334, 2003.
- [33] J. A. T. P. K. M. H. Tom Krupenkin, "Electrically tunable superhydrophobic nanostructured surfaces," *Bell Labs Technical Journal*, vol. 10, pp. 161-170, 2005.
- [34] A. Ahuja, J. A. Taylor, V. Lifton, A. A. Sidorenko, T. R. Salamon, E. J. Lobaton, P. Kolodner, and T. N. Krupenkin, "Nanonails: A Simple Geometrical Approach to Electrically Tunable Superhydrophobic Surfaces," *Langmuir*, vol. 24, pp. 9-14, 2008.
- [35] P. Bertrand, A. A. Jonas, and L. R. Legras, "Ultrathin polymer coatings by complexation of polyelectrolytes at interfaces: suitable materials, structure and properties," *Macromolecular Rapid Communications*, vol. 21, pp. 319-348, 2000.
- [36] G. Decher and J. B. Schlenoff, *Multilayer Thin Films: Sequential Assembly of Nanocomposite Materials*;: Wiley-VCH: Weinheim, 2003.
- [37] G. T. A. Kovacs, *Micromachined Transducers Sourcebook*, International Editions 2000 ed.: WCB/McGraw-Hill, 2000.
- [38] M. R. McNeely, M. K. Spute, N. A. Tusneem, and A. R. Oliphant, "Hydrophobic microfluidics," in *Proceedings of SPIE*, 1999, pp. 1-11.

- [39] D. S. Kim, K.-C. Lee, T. H. Kwon, and S. S. Lee, "Microchannel Filling Flow Considering Surface Tension Effect," *JOURNAL OF MICROMECHANICS AND MICROENGINEERING*, vol. 12, pp. 236-246, 2002.
- [40] M. S. Todd and R. Q. Stephen, "Microfluidics: Fluid physics at the nanoliter scale," *Reviews of Modern Physics*, vol. 77, p. 977, 2005.
- [41] T. Young, "An Essay on the Cohesion of Fluids," *Philosophical Transactions of the Royal Society of London*, vol. 95, pp. 65-87, 1805.
- [42] R. N. Wenzel, "Resistance of Solid Surfaces to Wetting by Water," *Ind. Eng. Chem.*, vol. 28, pp. 988-994, 1936.
- [43] A. B. D. Cassie and S. Baxter, "Wettability of Porous Surfaces," *Trans. Faraday Soc.*, vol. 40, pp. 546-551, 1944.
- [44] J. Bico, C. Marzolin, and D. Qu, "Pearl drops," *EPL (Europhysics Letters)*, p. 220, 1999.
- [45] N. A. Patankar, "On the Modeling of Hydrophobic Contact Angles on Rough Surfaces," *Langmuir*, vol. 19, pp. 1249-1253, 2003.
- [46] L. Zhai, F. C. Cebeci, R. E. Cohen, and M. F. Rubner, "Stable Superhydrophobic Coatings from Polyelectrolyte Multilayers," *Nano Letters*, vol. 4, pp. 1349-1353, 18 May 2004 2004.
- [47] G. Coppola, V. Striano, P. Ferraro, S. De Nicola, A. Finizio, G. Pierattini, and P. Maccagnani, "A Nondestructive Dynamic Characterization of a Microheater Through Digital Holographic Microscopy," *Microelectromechanical Systems, Journal of*, vol. 16, pp. 659-667, 2007.
- [48] M. Bachman and L. L. Wu, "Gold etch using potassium iodide solution," 2002.
- [49] K. R. Williams, K. Gupta, and M. Wasilik, "Etch rates for micromachining processing-Part II," *Microelectromechanical Systems, Journal of*, vol. 12, pp. 761-778, 2003.

- [50] J. Choi and M. F. Rubner, "Influence of the Degree of Ionization on Weak Polyelectrolyte Multilayer Assembly," *Macromolecules*, vol. 38, pp. 116-124, October 21 2004 2004.
- [51] L. K. Ista, S. Mendez, V. H. Perez-Luna, and G. P. Lopez, "Synthesis of Poly(N-isopropylacrylamide) on Initiator-Modified Self-Assembled Monolayers," *Langmuir*, vol. 17, pp. 2552-2555, May 1, 2001 2001.
- [52] G. M. Whitesides, "The origins and the future of microfluidics," *Nature*, vol. 442, pp. 368-373, 2006.
- [53] K. W. Oh and C. H. Ahn, "Review of Microvalves," *Journal of Micromechanics and Microengineering*, vol. 16, pp. R13-R39, 24 March 2006 2006.
- [54] A. Puntambekar, "Microfluidic Dispensers Based on Structurally Programmable Microfluidic Systems (sPROMs) and Their Applications for MicroTAS," in *Department of Electrical Engineering and Computer Engineering and Computer Science*. vol. Ph.D. Cincinnati: University of Cincinnati, 2003, p. 233.
- [55] D. J. Beebe, J. S. Moore, J. M. Bauer, Q. Yu, R. H. Liu, C. Devadoss, and B.-H. Jo, "Functional hydrogel structures for autonomous flow control inside microfluidic channels," *Nature*, vol. 404, pp. 588-590, 2000.
- [56] S. Daniel, M. K. Chaudhury, and J. C. Chen, "Fast Drop Movements Resulting from the Phase Change on a Gradient Surface," *Science*, vol. 291, pp. 633-636, January 26, 2001 2001.
- [57] R. Mohammadi, J. Wassink, and A. Amirfazli, "Effect of Surfactants on Wetting of Super-Hydrophobic Surfaces," *Langmuir*, vol. 20, pp. 9657-9662, 2004.
- [58] T. Arakawa, Y. Sato, T. Ueno, T. Funatsu, and S. Shoji, "Pinhole free Pyrex Glass Etching Using HF-H₂SO₄ Mixed Acid and its Applications for a PDMS Microflow System," in *Transducers'05 - The 13th International Conference on Solid-State Sensors, Actuators and Microsystems*, Seoul, Korea, 2005, pp. 1489-1492.
- [59] D. C. Duffy, C. J. McDonald, O. J. A. Schueller, and G. M. Whitesides, "Rapid Prototyping of Microfluidic Systems in Poly(dimethylsiloxane)," *Analytical Chemistry*, vol. 70, pp. 4974-4984, December 1 1998 1998.

- [60] B.-H. Jo, L. M. Van Lerberghe, K. M. Motsegood, and D. J. Beebe, "Three-Dimensional Micro-Channel Fabrication in Polydimethylsiloxane (PDMS) Elastomer," *Journal of Microelectromechanical Systems*, vol. 9, pp. 76-81, 2000.
- [61] M. Miwa, A. Nakajima, A. Fujishima, K. Hashimoto, and T. Watanabe, "Effects of the Surface Roughness on Sliding Angles of Water Droplets on Superhydrophobic Surfaces," *Langmuir*, vol. 16, pp. 5754-5760, 2000.
- [62] T. Nishino, M. Meguro, K. Nakamae, M. Matsushita, and Y. Ueda, "The Lowest Surface Free Energy Based on -CF₃ Alignment," *Langmuir*, vol. 15, pp. 4321-4323, 1999.
- [63] L. Zhai, M. C. Berg, F. C. Cebeci, Y. Kim, J. M. Milwid, M. F. Rubner, and R. E. Cohen, "Patterned Superhydrophobic Surfaces: Toward a Synthetic Mimic of the Namib Desert Beetle," *Nano Lett.*, vol. 6, pp. 1213-1217, 2006.
- [64] T. Thorsen, S. J. Maerkl, and S. R. Quake, "Microfluidic Large-Scale Integration," *Science*, vol. 298, pp. 580-584, October 18, 2002 2002.
- [65] "Young 4ever-the use of capillarity for passive flow handling in lab on a chip devices," *Lab on a Chip*, vol. 6, pp. 1405-1408, 2006.
- [66] J. Atencia and D. J. Beebe, "Controlled microfluidic interfaces," *Nature*, vol. 437, pp. 648-655, 2005.
- [67] E. M. Purcell, "Life at low Reynolds number," *American Journal of Physics*, vol. 45, pp. 3-11, 1977.
- [68] B. Zhao, J. S. Moore, and D. J. Beebe, "Surface-Directed Liquid Flow Inside Microchannels," *Science*, vol. 291, pp. 1023-1026, February 9, 2001 2001.
- [69] K. Haubert, T. Drier, and D. Beebe, "PDMS bonding by means of a portable, low-cost corona system," *Lab on a Chip*, vol. 6, pp. 1548-1549, 2006.
- [70] B.-C. Lin and Y.-C. Su, "On-demand Liquid-in-Liquid Droplet Metering and Fusion Utilizing Pneumatically-Actuated Membrane-Type Valves," *Journal of Micromechanics and Microengineering*, vol. Provisionally scheduled for Sept 2008, 2008.

- [71] H. A. Stone, A. D. Stroock, and A. Ajdari, "ENGINEERING FLOWS IN SMALL DEVICES Microfluidics Toward a Lab-on-a-Chip," *Annual Review of Fluid Mechanics*, vol. 36, pp. 381-411, 2004.
- [72] A. Gunther and K. F. Jensen, "Multiphase microfluidics: from flow characteristics to chemical and materials synthesis," *Lab on a Chip*, vol. 6, pp. 1487-1503, 2006.
- [73] "Viscosity," http://en.wikipedia.org/wiki/Dynamic_viscosity, 2008.
- [74] A. W. Adamson and A. P. Gast, *Physical Chemistry of Surfaces*, 1997 ed. vol. 1: New York John Wiley & Sons, Inc. (US), 1997.
- [75] H.-J. Butt, K. Graf, and M. Kappl, *Physics and Chemistry of Interfaces* vol. 1: Wiley-VCH, 2003.
- [76] J. Pellicer, V. Garcia-Morales, L. Guanter, M. J. Hernandez, and M. Dolz, "On the experimental values of the water surface tension used in some textbooks," *American Journal of Physics*, vol. 70, pp. 705-709, 2002.
- [77] B. Zhao, J. S. Moore, and D. J. Beebe, "Pressure-Sensitive Microfluidic Gates Fabricated by Patterning Surface Free Energies Inside Microchannels," *Langmuir*, vol. 19, pp. 1873-1879, 2003.
- [78] C. Matthews, *Asme Engineer's Data Book*, Second Edition ed.: ASME Press, 2005.
- [79] A. Puntambekar, J.-W. Choi, C. H. Ahn, S. Kim, and V. Makhijani, "Fixed-Volume Metering Microdispenser Module," *Lab on a Chip*, vol. 2, pp. 213-218, 2002.
- [80] L. Hao, E. O. Leonidas, A. Orlando, and F. Millicent, "Design and fabrication of a multilayer micro-/nanofluidic device with an electrically driven nanovalve," 2008, pp. 752-756.

PUBLICATIONS AND PRESENTATIONS

- **G. Londe**, A. Chunder, A. Wesser, L. Zhai and H. J. Cho, “Microfluidic Valves Based On Superhydrophobic Nanostructures And Switchable Thermosensitive Surface For Lab-on-a-chip (LOC) Systems”, *Sensors and Actuators B: Chemical*, Vol. 132, No. 2, 16 June 2008, pp. 431 – 438.
- **G. Londe**, A. Wesser, L. Zhai, H. J. Cho, A. Chunder and S. Subbarao “A Passive Microfluidic Valve Using Superhydrophilic/hydrophobic nanostructures for Lab-on-a-chip (LOC) systems”, *Transducers 07*, The 14th International Conference on Solid-State Sensors, Actuators and Microsystems, June 10 – 14, 2007, Lyon, France, Vol. 2, pp. 1801 – 1804.
- **Ghanashyam Londe**, Anindarupa Chunder, Lei Zhai and Hyoung J. Cho, “A Nanostructured Thermosensitive Smart Surface With Integrated Microheater for Wettability Control”, *Proceedings of IMECE2008*, 2008 ASME International Mechanical Engineering Congress and Exposition, October 31 – November 6, 2008, Boston, Massachusetts, USA (accepted).
- **Ghanashyam Londe**, Hyoung Jin Cho, Arum Ham, Chapter “MEMS for Nanotechnology” for the book “Functional Nanostructures: Processing, Characterization and Applications”, Springer Publications, edited by Dr. Sudipta Seal, ISBN: 978-0-387-35463-7.
- **G. Londe**, A. Chunder, L. Zhai and H. J. Cho, “An Analytical Model for the Wettability Switching Characteristic of a Nanostructured Thermoresponsive Surface”, *Applied Physics Letters* (submitted).
- P. Zhang, **G. Londe**, J. Sung, E. Johnson, M. Lee and H. J. Cho, “Microlens Fabrication Using an Etched Glass Master”, *Microsystems Technology*, Feb. 2007, Vol. 13, Nos. 3 – 4, pp. 339 – 342.
- Chunder, **G. Londe**, K. Etcheverry, H. J. Cho, L. Zhai, “Temperature Switchable Superhydrophobic/Hydrophilic Planar Valves in Microfluidic Channels”, 2008 Annual Joint Symposium & Exhibition Florida Chapter of the AVS Science and Technology Society (FLAVS) and Florida Society for Microscopy (FSM), March 10 – 11, 2008, Orlando, FL.
- Sameer Deshpande, **Ghanashyam Londe**, Hyoung Cho and Sudipta Seal, “Dimensionally Encoded Nanosensor for Room Temperature Hydrogen Detection”, 2007 Nanomaterials: Fabrication, Properties and Applications, TMS 2007 Annual Meeting & Exhibition, Feb. 25 – Mar. 1, 2007, Orlando, FL.

- Peng Zhang, **Ghanashyam Londe**, Jinwon Sung, Eric Johnson, Moo Sung Lee & Hyoung Jin Cho, “Microlens Fabrication Using an Etched Glass Master”, Book of Abstract, The 6th International Workshop on High Aspect Ratio Micro Structure Technology (HARMST 2005), June 10 – 13, 2005, Gyeongju, Korea, pp.246 – 247.
- Anindarupa Chunder, Kenneth Etcheverry, **Ghanashyam Londe**, Hyoung J. Cho, Lei Zhai, “Conformal Switchable Superhydrophobic/Hydrophilic Surfaces for Microscale Flow Control”, Colloids and Surfaces A: Physicochemical and Engineering Aspects (accepted).
- Deshpande, S.; Karakoti, A.; **Londe, G.**; Cho, H.J. and Seal, S., “Room Temperature Hydrogen Detection Using 1-D Nanostructured Tin Oxide Sensor”, Journal of Nanoscience and Nanotechnology, Sept. 2007, Vol. 7, No. 9, pp. 3354 – 3357(4).
- S. Deshpande, A. Karakoti, **G. Londe**, H. Cho and S. Seal, “Fabrication of Tin Oxide Nanowire Based Nano-Micro Sensor for Room Temperature Hydrogen Detection”, 53rd AVS International Symposium and Exhibition, Nov. 12 – 17, 2006, San Francisco, CA.
- Sandra Furterer, Abeer Sharawi, Cesar Casanas, **Ghanashyam Londe**, Louis Linde Jr. and Tareq Ahram, “Six Sigma Project – Improving Web Development and Design Processes”, 12th Annual Conference on Industry Engineering and Management Systems (IEMS), March 13 – 15, 2006, Cocoa Beach, FL.